DEVELOPMENTAL NEUROSCIENCE

FOXG1 sequentially orchestrates subtype specification of postmitotic cortical projection neurons

Junhua Liu[1], Mengjie Yang[1], Mingzhao Su[1], Bin Liu[1], Kaixing Zhou[1], Congli Sun[1], Ru Ba[1], Baocong Yu[1], Baoshen Zhang[1], Zhe Zhang[1], Wenxin Fan[2], Kun Wang[1], Min Zhong[1], Junhai Han[2], Chunjie Zhao[1]*

The mammalian neocortex is a highly organized six-layered structure with four major cortical neuron subtypes: corticothalamic projection neurons (CThPNs), subcerebral projection neurons (SCPNs), deep callosal projection neurons (CPNs), and superficial CPNs. Here, careful examination of multiple conditional knockout model mouse lines showed that the transcription factor FOXG1 functions as a master regulator of postmitotic cortical neuron specification and found that mice lacking functional FOXG1 exhibited projection deficits. Before embryonic day 14.5 (E14.5), FOXG1 enforces deep CPN identity in postmitotic neurons by activating *Satb2* but repressing *Bcl11b* and *Tbr1*. After E14.5, FOXG1 exerts specification functions in distinct layers via differential regulation of *Bcl11b* and *Tbr1*, including specification of superficial versus deep CPNs and enforcement of CThPN identity. FOXG1 controls CThPN versus SCPN fate by fine-tuning *Fezf2* levels through diverse interactions with multiple SOX family proteins. Thus, our study supports a developmental model to explain the postmitotic specification of four cortical projection neuron subtypes and sheds light on neuropathogenesis.

INTRODUCTION

The mammalian cortical projection neurons are grossly classified into two main groups, the corticofugal neurons (CFuNs) and the callosal neurons (CPNs). CFuNs are further divided into layer 6 (L6) corticothalamic neurons (CThPNs) that project to the thalamus, and L5 subcerebral neurons (SCPNs) that project to the brainstem and the spinal cord (*1*). Clinical research has established that dysfunction of CFuNs results in perceptual-motor dysfunctions common to diverse developmental disorders (*2*–*4*). CPNs including deep and superficial CPNs function in connecting the two cerebral hemispheres and coordinate many advanced brain functions (*5*–*7*). During neurogenesis, cortical projection neurons are generated in sequential but partially overlapping waves. Deep layer neurons including CThPNs, SCPNs, and deep CPNs arise at early corticogenesis, whereas neurons positioned in more superficial layers are produced later (*8*). Understanding the mechanisms underlying cortical subtype specification will almost certainly help resolve the etiopathology of numerous neurological disorders.

The postmitotic acquisition and maintenance of subtype identities are coordinated by the sequential activation/repression of gene expression programs; these programs are largely mediated by stage- and subtype-specific transcription factors. Four transcription factors—TBR1 (*T-box transcription factors Tbr1*), FEZF2 (*the zinc finger transcription factors Fezf2*)/BCL11B (*B-cell leukemia/lymphoma 11B*), and SATB2 (*chromatin-remodeling protein Satb2*)—have been reported as crucial for postmitotic specification during neurogenesis; these proteins respectively determine the identities of CThPNs, SCPNs, and deep/superficial CPNs (*9*–*11*). During early corticogenesis, the respective levels of initially coexpressed regulators in newborn cortical neurons (including TBR1, FEZF2, BCL11B, and SATB2) are subsequently altered as the distinct neuron subtypes are specified (*8*, *12*). Moreover, it has been shown that these regulators can physically interact with each other to shape the final subtype identity. Disruption of any one of these regulators leads to aberrant cortical projection neuron subtype identities (*13*–*19*). Multiple studies have demonstrated that various SOX family members are also required for specifying cortical neuron subtypes (*20*–*22*). Although there have been true breakthrough advances in our understanding in recent years, much remains unknown about the activation/repression transcriptional networks that spatiotemporally control the proper development of postmitotic cortical projection neurons.

FOXG1, a member of the Forkhead-box family of transcription factors, has been linked to a broad array of developmental processes (*23*–*28*). Clinically, patients with FOXG1-related syndrome suffer from severe mixed dyskinesia and cognitive deficits and exhibit serious corpus callosum dysplasia (*29*), strongly suggesting a possible role of FOXG1 in subtype specification. In the present study, we used a combination of conditional genetic disruption at postmitotic stages, cell tracing, immunostaining, in situ RNA hybridization, and chromatin immunoprecipitation (ChIP) methods, which enabled our demonstration of FOXG1 as a major spatiotemporal regulator of postmitotic projection neuron subtype specification. This protein variously controls both induction and repression programs, doing so in both developmental stage–specific and neuron subtype–specific manners.

RESULTS

Dynamic expression of transcription factors defines impactful regulatory windows during postmitotic cortical neuron specification

To investigate postmitotic specification of cortical projection neurons, we first carefully profiled the TBR1, BCL11B, and SATB2 levels during embryonic day 12.5 (E12.5) to postnatal day 0 (P0). At E12.5,

[1]Key Laboratory of Developmental Genes and Human Diseases, Ministry of Education, School of Medicine, Southeast University, Nanjing 210009, China. [2]Key Laboratory of Developmental Genes and Human Diseases, Ministry of Education, School of Life Science and Technology, Southeast University, Nanjing 210009, China.
*Corresponding author. Email: zhaocj@seu.edu.cn

TBR1 and BCL11B were highly coexpressed at the cortical plate (CP); this TBR1^{high}BCL11B^{high} pattern suggests that these neurons have acquired CFuN characteristics after exiting the cell cycle (fig. S1A). From E14.5 onward, we observed gradual decreases for TBR1 expression in SCPNs and for BCL11B expression in CThPNs, respectively, leading to L5 BCL11B^{high}TBR1^{low} SCPN and L6 BCL11B^{low}TBR1^{high} CThPN patterns at P0 (fig. S1A).

Consistent with a previous report (*14*), SATB2 was not detectable at the E12.5 cortex (fig. S1, B and C). At E14.5, we found that SATB2 was mainly expressed in deep CPNs most present in the intermediate zone (IZ), as well as in a small proportion in the CP. These SATB2^{+} deep CPNs coexpressed low levels of BCL11B and TBR1, exhibiting a SATB2^{high}TBR1^{low}BCL11B^{low} pattern (fig. S1, B and C). By E16.5, most of the deep CPNs had already migrated to the deep layer of the CP, and this migration was accompanied by a gradual down-regulation of BCL11B and TBR1. Many superficial CPNs expressing SATB2 were present in both the superficial layer and the IZ, and it was notable that BCL11B was undetectable in superficial CPNs at this stage (fig. S1, B and C).

At P0, SATB2 was highly expressed in both deep and superficial CPNs, and these cells all coexpressed a low level of TBR1 (fig. S1, B and C). BCL11B was undetectable in the majority of P0 CPNs (fig. S1, B and C). As summarized in fig. S1D, these dynamic expression patterns in each of the four cortical projection neuron subtypes suggest that acquisition of CFuN identity is already initiated at E12.5, that further specification of CFuNs toward CThPNs or SCPNs is apparently initiated around E14.5, and that distinct mechanisms function to specify the two CPN subtypes.

We also detected a possible role of FOXG1 in postmitotic subtype specification. That is, we observed strong expression of FOXG1 in CFuNs at all tested stages (i.e., matching expression patterns of BCL11B and TBR1) (fig. S2, A and B), as well as FOXG1 coexpression with SATB2 in developing deep and superficial CPNs (fig. S2C). Quantification of fluorescence intensity showed that at E14.5, FOXG1 expression level in SATB2^{+} deep CPNs was lower than that in BCL11B^{+} CFuNs in the CP (fig. S2D). As development proceeded, at E16.5, the level of FOXG1 in SATB2^{+} deep CPNs became higher than that in BCL11B^{+} SCPNs in the deep layer (fig. S2E).

FOXG1 is required for both deep and superficial postmitotic CPN identity and for progression beyond the CFuN state

Next, *Foxg1* was deleted by crossing the *Foxg1$^{fl/fl}$* line with *NEX-Cre*, in which CRE (Cyclization Recombination Enzyme)–mediated recombination occurs in postmitotic cortical neurons from E11.5 onward (Fig. 1A) (*30*). FOXG1 was highly expressed in control but was almost undetectable in *NEX-Cre;Foxg1* conditional knockout (cKO) postmitotic neurons (Fig. 1B), supporting efficient deletion. For control mice at E14.5, the CP was extensively populated with TBR1^{high}BCL11B^{high} CFuNs as well as a small proportion of SATB2^{high}TBR1^{low}BCL11B^{low} deep CPNs. Rich populations of deep CPNs were located in the IZ (Fig. 1C). In contrast, for the *NEX-Cre;Foxg1* cKO mice, TBR1^{high}BCL11B^{high} CFuNs populated the entire cortex including the CP and the IZ. The SATB2 levels in these mice were also notably reduced, and no SATB2^{high}TBR1^{low}BCL11B^{low} deep CPNs were detectable (Fig. 1C). Quantitative analysis of each subtype throughout the entire cortex revealed a marked and significant decrease in the number of SATB2^{high} CPNs in the *NEX-Cre;Foxg1* cKO mice, and this was accompanied by a remarkably increased number of BCL11B^{high}TBR1^{high} CFuNs (Fig. 1G), results suggesting that *Foxg1* deletion after E11.5 causes extensive loss of deep CPNs.

At E16.5, SATB2^{high} CPNs were present in both the superficial and deep layers in control mice (Fig. 1D). In *NEX-Cre;Foxg1* cKO mice, few SATB2^{high} CPNs were observed throughout the entire cortex, and only a very low level of SATB2 was detected in the IZ (Fig. 1D). Previous studies have reported that *Foxg1* deletion leads to migration defects and a decrease in the number of SATB2^{high} CPNs (*24*, *25*); so, it is plausible that the SATB2^{low} neurons we detected in the *NEX-Cre;Foxg1* cKO IZ might represent a mixed population comprising both deep and superficial CPNs. Consistent with this idea, note that we observed increased TBR1 levels in both the upper IZ (where putative deep CPNs are positioned) and the lower IZ (superficial CPN site), whereas BCL11B accumulation was only detected in the upper IZ but not the lower IZ (Fig. 1D). Last, this examination of the *NEX-Cre;Foxg1* cKO cortex revealed that the significant reduction of SATB2^{high} CPNs was accompanied by a significant increase in BCL11B^{high}TBR1^{high} CFuNs in the entire cortex (Fig. 1H). These findings collectively demonstrate that FOXG1 is required for both deep and superficial CPN identities. Moreover, it is clear that *Foxg1* deletion results in the accumulation of both TBR1 and BCL11B in deep CPNs, but only results in TBR1 accumulation in superficial CPNs.

Consistently, at P0, almost all of the neurons at the *NEX-Cre;Foxg1* cKO CP displayed a BCL11B^{high}TBR1^{high} CFuN pattern, with few SATB2^{high} CPNs observed (Fig. 1, E and I), indicating a shift of deep CPNs toward CFuNs. Moreover, the TBR1 level was obviously increased throughout the IZ at P0, while BCL11B was only accumulated in the upper IZ, indicating that two distinct mechanisms are involved in FOXG1's specification of deep CPNs and superficial CPNs. Moreover, TBR1^{high}BCL11B^{low} CThPNs and BCL11B^{high}TBR1^{low} SCPNs were not detected in the *NEX-Cre;Foxg1* cKO cortex. To further characterize neuron identities, we performed immunostaining with additional subtype-specific markers at P0. We stained *NEX-Cre;Foxg1* cKO brains for FOG2 (Friend of GATA-2) (reported as specifically expressed in CFuNs) (*31*, *32*) and for the commonly used CPN marker CUX1 (cut-like homeobox 1) (*33*). In *NEX-Cre;Foxg1* cKO brains, the level of FOG2 was significantly increased and displayed a similar abnormal accumulation pattern with TBR1 and BCL11B (Fig. 1F). Similar to SATB2, CUX1 was significantly reduced in CPNs in *NEX-Cre;Foxg1* cKO mice (Fig. 1F). These data collectively support that specification of FOXG1-deficient neurons is arrested at the CFuN stage (i.e., unable to progress toward SCPN or CThPN fates).

Foxg1 deletion at E14.5 impairs the specification of cortical neurons including CThPNs, SCPNs, deep CPNs, and superficial CPNs

The arrested CFuN specification and lost CPNs in *NEX-Cre;Foxg1* cKO mice precluded the investigation of the subsequent specification of the four neuron subtypes in these mice; we therefore used tamoxifen (TM) induction of *CAG-CreER* mice to disrupt *Foxg1* at E14.5 (Fig. 2, A and B). At P0, compared with successful specification of L5 BCL11B^{high}TBR1^{low} SCPNs and L6 TBR1^{high}BCL11B^{low} CThPNs in control cortices, the TM-induced *CAG-CreER;Foxg1* cKO mice did not display BCL11B down-regulation in TBR1^{high} CThPNs, whereas TBR1 expression was normally down-regulated in *Foxg1*-deficient SCPNs (Fig. 2C). Consistent with these observations, quantitative analysis showed the number of TBR1^{high} neurons in the deep layer did not differ between control and *CAG-CreER;Foxg1*

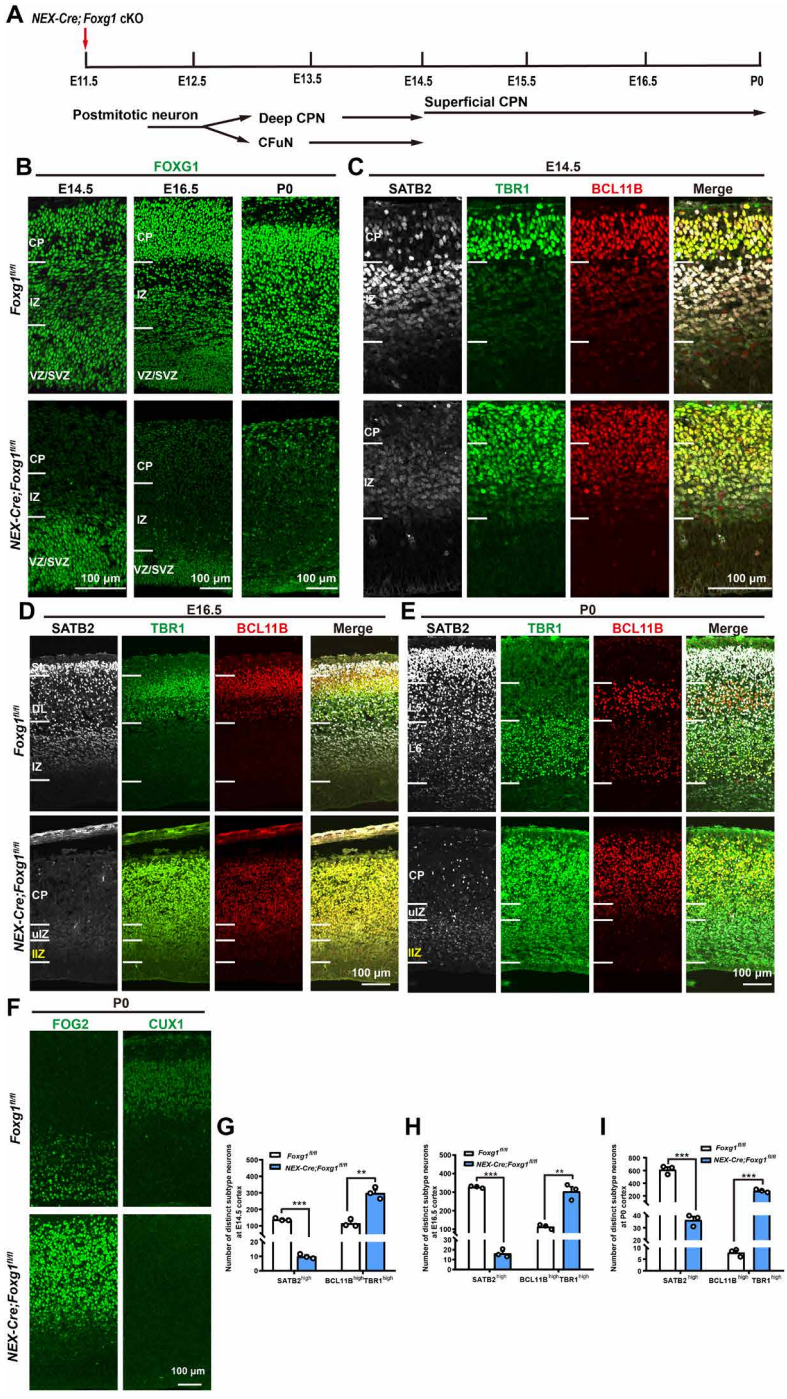

Fig. 1. Deletion of *Foxg1* from E11.5 onward leads to lost CPN identity and an arrested CFuN state. (**A**) Schematic of *Foxg1* disruption strategy in postmitotic neurons at E11.5. (**B**) Immunostaining showing that FOXG1 was efficiently disrupted. (**C**) Triple immunostaining against SATB2, TBR1, and BCL11B at E14.5, revealing markedly decreased SATB2 levels at the CP and IZ, and increased levels of BCL11B and TBR1 in *NEX-Cre;Foxg1* cKO IZ. (**D**) Triple immunostaining against SATB2, TBR1, and BCL11B at E16.5, showing that the *NEX-Cre;Foxg1* cKO cortex has many neurons expressing low SATB2 levels in the IZ. The whole CP and upper IZ were all occupied with TBR1^{high}BCL11B^{high} neurons. In the lower IZ, TBR1 but not BCL11B levels were increased in *NEX-Cre;Foxg1* cKO mice. (**E**) Triple immunostaining against SATB2, TBR1, and BCL11B at P0 showing that in the *NEX-Cre;Foxg1* cKO cortex, few SATB2^{high} CPNs were detected and that most postmitotic neurons in the CP were arrested at the TBR1^{high}BCL11B^{high} CFuN stage. In IZ, TBR1 but not BCL11B was obviously up-regulated in SATB2^{low} superficial CPNs. (**F**) Immunostaining against FOG2 and CUX1 at P0, showing that the level of FOG2 was increased while the CUX1 level was remarkably reduced in the CP of *NEX-Cre;Foxg1* cKO mice. (**G** to **I**) Quantitative analysis showing a reduction in SATB2^{high} CPNs but an increase in BCL11B^{high}TBR1^{high} CFuNs at E14.5 (G), a remarkable reduction in SATB2^{high} CPNs yet an increase in BCL11B^{high}TBR1^{high} CFuNs at E16.5 (H), and reduced SATB2^{high} CPN numbers but increased BCL11B^{high}TBR1^{high} CFuN numbers at P0 (I). Data are presented as means ± SEM; $n = 3$, multiple Student's t test with Bonferroni correction. $^{**}P < 0.01$; $^{***}P < 0.001$. uIZ, upper intermediate zone; lIZ, lower intermediate zone; VZ, ventricular zone; SVZ, subventricular zone; DL, deep layer; SL, superficial layer.

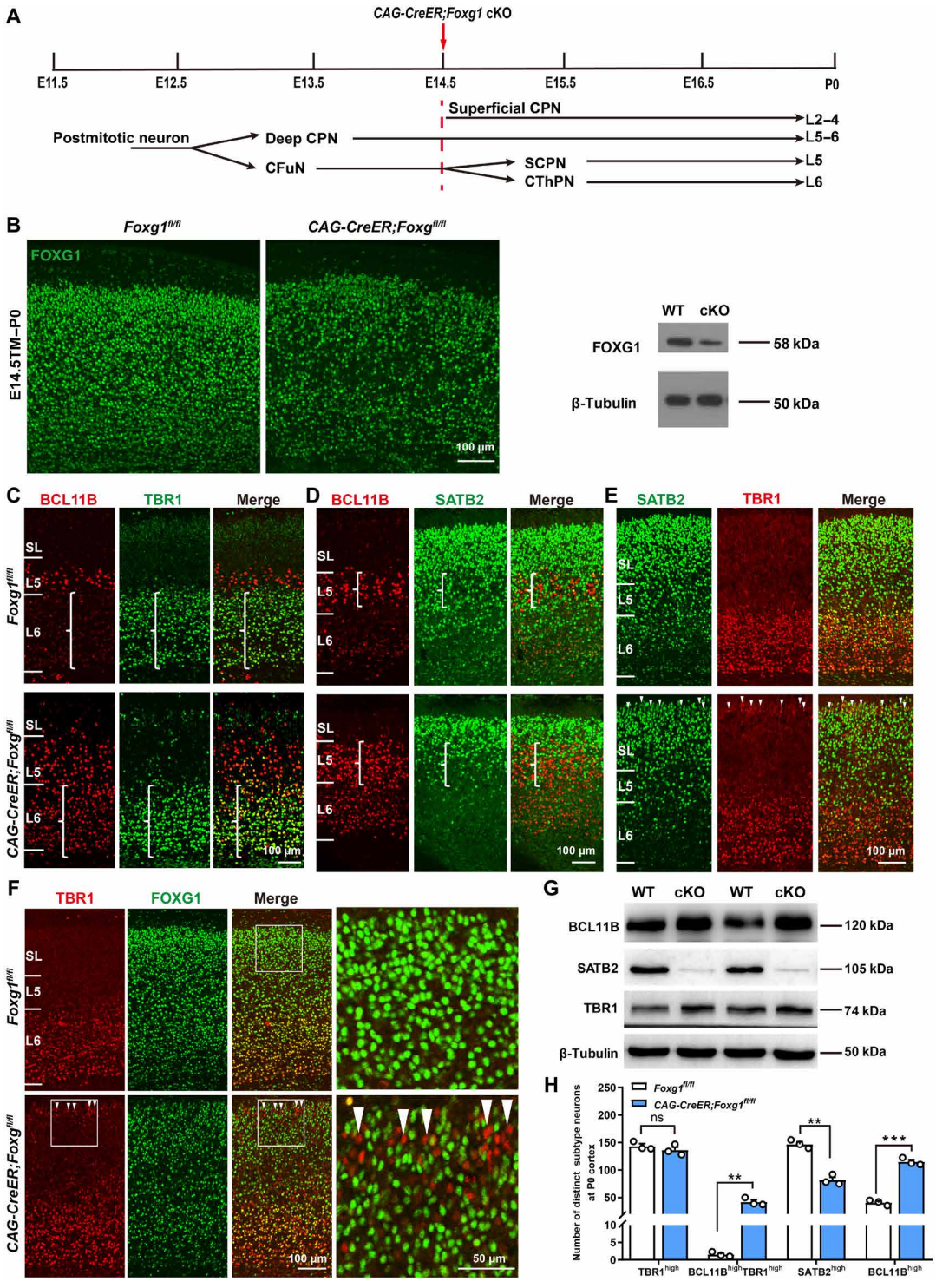

Fig. 2. Deletion of *Foxg1* from E14.5 onward impairs the specification of CThPNs, deep CPNs, and superficial CPNs. (**A**) Schematic of *Foxg1* disruption strategy at E14.5. (**B**) Immunostaining and Western blot using P0 cortex, showing that *Foxg1* was efficiently disrupted. (**C** to **E**) Double immunostaining at P0, showing failed BCL11B down-regulation in TBR1^{high} CThPNs (C), decreased SATB2^{high} deep CPNs and increased BCL11B^{high} neurons in L5 (D), and TBR1 up-regulation in SATB2^{low} superficial CPNs in *CAG-CreER;Foxg1$^{fl/fl}$* cKO cortices (E) (arrowheads). (**F**) Double immunostaining of TBR1 and FOXG1 at P0, showing up-regulation of TBR1 in FOXG1-deficient superficial CPNs (arrowheads). (**G**) Western blot of P0 cortex, showing increased levels of BCL11B and TBR1 and decreased levels of SATB2 in *CAG-CreER;Foxg1* cKO mice. (**H**) Quantitative analysis showing an increase in BCL11B^{high}TBR1^{high} and BCL11B^{high} neurons yet a reduction in SATB2^{high} neurons in the deep layer at P0 in *CAG-CreER;Foxg1* cKO mice. There were no obvious differences in the number of TBR1^{high} neurons between control and *CAG-CreER;Foxg1* cKO mice. Data are presented as means ± SEM; $n = 3$, multiple *t* test with Bonferroni correction. $^{**}P < 0.01$; $^{***}P < 0.001$; ns, not significant. WT, wild type.

cKO cortices, but the number of BCL11B^{high}TBR1^{high} neurons of *CAG-CreER;Foxg1* cKO mice was significantly increased (Fig. 2H).

We next examined the specification of deep and superficial CPNs. Immunostaining against BCL11B was used to demarcate the superficial and deep layers. Compared with controls, the number of SATB2^{high} *CAG-CreER;Foxg1* cKO deep CPNs was significantly reduced at P0, whereas the number of BCL11B^{high} SCPNs was remarkably increased (Fig. 2, D and H). For the superficial CPNs in the cKO mice, the TBR1 level was increased (Fig. 2E). Note that staining against TBR1 and FOXG1 confirmed that these superficial CPNs were FOXG1 deficient (Fig. 2F), and Western blotting confirmed the up-regulation of BCL11B and TBR1 and down-regulation of SATB2 in P0 *CAG-CreER;Foxg1* cKO cortices (Fig. 2G). Quantitative analysis of subtypes in the deep layer showed a marked decrease in the number of SATB2^{high} CPNs that was accompanied by a nearly threefold increase in BCL11B^{high} SCPNs in the *CAG-CreER;Foxg1* cKO cortex (Fig. 2H). Thus, disruption of *Foxg1* at E14.5 leads to failed down-regulation of BCL11B in CThPNs, up-regulation of TBR1 in superficial CPNs, loss of deep CPNs, and an increase in the number of SCPNs.

Cell tracing reveals that *Foxg1* cKO at E11.5 both forces deep CPNs into a CFuN fate and impairs superficial CPN identity

Deep CPNs emerge at the same developmental stage as CFuNs (E12.5 to E14.5) (*8*, *34*, *35*). CFuNs express BCL11B and TBR1 at high levels, while in deep CPNs, *Bcl11b* and *Tbr1* are suppressed but *Satb2* is activated. We then performed a "birth-dating" experiment in which 5-bromo-2′-deoxyuridine (BrdU) was administered to pregnant mice at E12.5 and E13.5 to label CThPNs and SCPNs/deep CPNs, respectively. The proportions of distinct subtypes specified from E12.5-born neurons were detected at P0 by quantification of TBR1^{high}BrdU^{+}, BCL11B^{high}BrdU^{+}, and SATB2^{high}BrdU^{+} neurons among total BrdU^{+} neurons; we detected no difference in the proportion of TBR1^{high}BrdU^{+}/BrdU^{+} neurons in the cortex of *NEX-Cre;Foxg1* cKO and control mice (Fig. 3, A and G). Because only a very small number of SATB2^{+} CPNs are born at E12.5 (*34*–*36*), the percentages of SATB2^{+}BrdU^{+} cells among total BrdU^{+} neurons were very low in both control and *NEX-Cre;Foxg1* cKO mice (Fig. 3, A and G). Triple staining showed BCL11B was highly coexpressed in TBR1^{high}BrdU^{+} neurons in *NEX-Cre;Foxg1* cKO mice but not in control mice (Fig. 3B), and the proportion of BCL11B^{high}BrdU^{+}/BrdU^{+} neurons was significantly increased, reaching a level nearly equal to that of TBR1^{high}BrdU^{+}/BrdU^{+} neurons in *NEX-Cre;Foxg1* cKO mice (Fig. 3H). These findings demonstrate an arrested CFuN state upon loss of *Foxg1*.

As for E13.5-born neurons, BCL11B^{high}BrdU^{+} and SATB2^{high}BrdU^{+} neurons represented SCPNs and deep CPNs, respectively. The proportion of SATB2^{high}BrdU^{+}/BrdU^{+} neurons was sharply reduced in *NEX-Cre;Foxg1* cKO mice compared with control at P0 (Fig. 3, C and H). Moreover, this reduction was accompanied by obvious increases in both the proportion of BCL11B^{high}BrdU^{+}/BrdU^{+} neurons and the proportion of TBR1^{high}BrdU^{+}/BrdU^{+} neurons in *NEX-Cre;Foxg1* cKO mice (Fig. 3, D and H). Together, these results showing that deletion of *Foxg1* causes deep CPNs to develop into CFuNs provide direct evidence that *Foxg1* functions to specify deep CPN identity, apparently by somehow prohibiting a CFuN developmental trajectory.

We also performed a birth-dating experiment at E15.5 to trace superficial CPNs in *NEX-Cre;Foxg1* cKO mice at P2. In the control cortices, SATB2^{high}BrdU^{+} CPNs populated the superficial layer (Fig. 3E). However, there were no SATB2^{high}BrdU^{+} CPNs in *NEX-Cre;Foxg1* cKO cortices, and E15.5-born BrdU^{+} neurons mainly accumulated in the IZ, with SATB2 staining very weak (Fig. 3E). To confirm the arrest of superficial CPNs in the IZ, we costained against SATB2 and PAX6 or TBR2 in *NEX-Cre;Foxg1* cKO cortices. As expected, no colocalization for SATB2 with any of these two proteins was detected (fig. S4, A and B). Moreover, costaining showed that the majority of E15.5-born BrdU^{+} cells did not express PAX6 or TBR2 in the *NEX-Cre;Foxg1* cKO IZ, demonstrating that these cells arrested in the IZ were not intermediate progenitors (fig. S4, C and D). Together, our results provide direct evidence that *Foxg1* is required to specify superficial CPN identity. In the *NEX-Cre;Foxg1* cKO IZ, the TBR1 level in BrdU^{+} neurons was increased to an intermediate level. Moreover, the proportion of TBR1^{medium}BrdU^{+}/BrdU^{+} neurons in *NEX-Cre;Foxg1* cKO cortices was significantly increased compared with control mice (Fig. 3, E and I). Thus, lacking *Foxg1*, TBR1 is up-regulated in E15.5-born superficial CPNs. Note that BCL11B was undetectable in E15.5-born BrdU^{+} neurons in either control or *NEX-Cre;Foxg1* cKO mice (Fig. 3, F and I), suggesting that FOXG1's regulation of superficial CPN specification may not involve BCL11B.

We next deleted *Foxg1* at E12.5 using in utero electroporation to deliver *pNeuroD1-Cre-GFP* (*37*) into the *Foxg1$^{fl/fl}$* mice. In addition to postmitotic neurons, *NeuroD1* promoter can also drive gene expression in a subset of intermediate progenitors (*38*); thus, at E18.5, green fluorescent protein (GFP) labeled both E12.5 postmitotic deep neurons and superficial CPNs, which derived from intermediate progenitors (fig. S3, A and B). In *pNeuroD1-Cre-GFP;Foxg1$^{fl/fl}$* cortices, one group of GFP^{+} neurons was detected near the deep layer in which SATB2 was undetectable, while both BCL11B and TBR1 were accumulated (fig. S3, A and B); the other group of GFP^{+} neurons that represents superficial CPNs with migration defects was arrested in the lower IZ. Moreover, SATB2 was undetectable in these neurons, and only TBR1 but not BCL11B was up-regulated (fig. S3, A and B). These results are in line with the observations in *NEX-Cre;Foxg1* cKO mice (Fig. 1, C to E) and further suggest that *Foxg1* functions to specify both deep and superficial CPN identities and controls the CFuN developmental trajectory.

Cell tracing reveals that *Foxg1* cKO at E14.5 both increases BCL11B accumulation in CThPNs and forces deep CPNs into an SCPN fate

To trace the developmental trajectories of deep CPNs and CFuNs toward CThPNs or SCPNs from E14.5 onward, we performed cell tracing experiments with *CAG-CreER;Foxg1* cKO mice. BrdU was administered at E12.5 or E13.5 to label CThPNs and SCPNs/deep CPNs, respectively, followed by TM induction at E14.5 to ensure that *Foxg1* was postmitotically disrupted in BrdU^{+} neurons. Among BrdU^{+} neurons born at E12.5, in *CAG-CreER;Foxg1* cKO mice, TBR1^{high}BrdU^{+} CThPNs abnormally expressed high-level BCL11B (fig. S5A); the proportion of BCL11B^{high} BrdU^{+}/BrdU^{+} neurons was significantly high in cKO compared with the control cortex, and the proportion of TBR1^{high}BrdU^{+}/BrdU^{+} neurons was comparable (fig. S5C). This result directly demonstrated that FOXG1 may repress BCL11B in CThPNs.

Among BrdU^{+} neurons born at E13.5, the number of BCL11B^{high}BrdU^{+} neurons was remarkably increased (fig. S5B), and this increase was accompanied by a decrease in the proportion of SATB2^{high}BrdU^{+}/BrdU^{+}

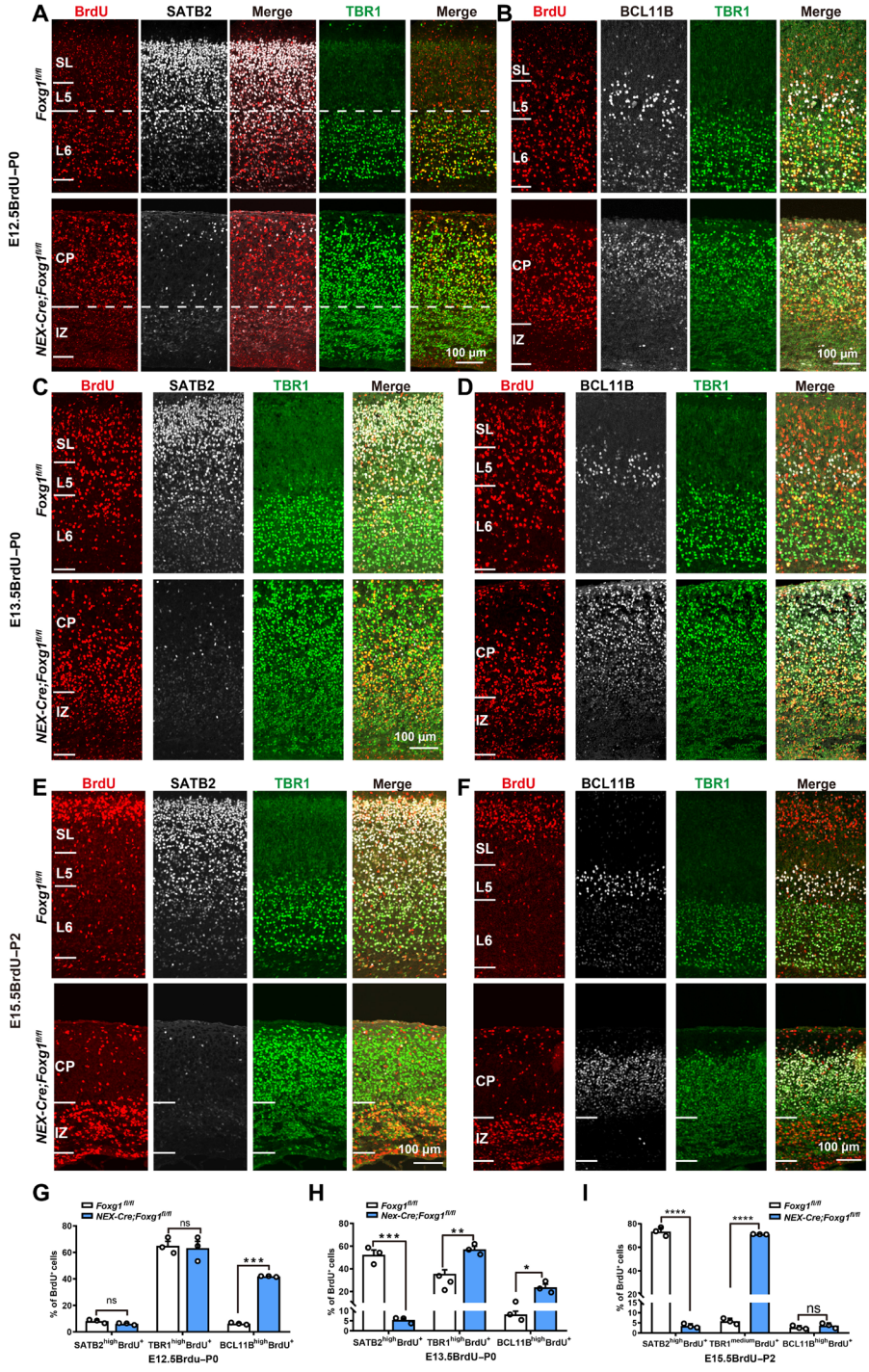

Fig. 3. Cell tracing indicated deep CPNs developed into CFuNs in *NEX-Cre;Foxg1* cKO mice. (**A**) Immunostaining showing that most E12.5-born neurons in control mice are TBR1^{high} CThPNs and positioned in L6; in cKO mice, TBR1^{high} CThPNs are dispersed throughout the CP. Few SATB^{high}BrdU^{+} neurons were born at E12.5 in either control or cKO mice. (**B**) Failed down-regulation of BCL11B in E12.5-born TBR1^{high}BrdU^{+} CThPNs in cKO CP. (**C**) Immunostaining tracing E13.5-born neurons, showing a significant reduction in SATB2^{high}BrdU^{+} neurons and an increase in TBR1^{high}BrdU^{+} neurons in cKO mice. (**D**) E13.5-born BrdU^{+} neurons have strong BCL11B expression in control L5, whereas they express high levels of both TBR1 and BCL11B in cKO mice. (**E**) E15.5-born neurons with strong SATB2 expression are positioned in the control superficial layer. In the cKO CP, BrdU^{+} neurons were restricted to the IZ and expressed some TBR1;, few of them expressed SATB2. (**F**) No BCL11B was detected in E15.5-born BrdU^{+} neurons neither in control nor in cKO mice. (**G** to **I**) Quantitative analysis showing in cKO mice an increased percentage of BCL11B^{high}BrdU^{+} neurons and unchanged percentages of SATB2^{high} BrdU^{+} neurons and TBR1^{high}BrdU^{+} neurons among E12.5-born neurons (G). A decreased percentage of SATB2^{high}BrdU^{+} neurons and increased percentages of TBR1^{high}BrdU^{+} neurons and BCL11B^{high}BrdU^{+} neurons among E13.5-born neurons (H). A sharp decrease in the percentage of SATB2^{high} BrdU^{+} neurons and an increase in the percentage of TBR1^{medium}BrdU^{+} neurons among E15.5-born neurons. Few BCL11B^{high}BrdU^{+} neurons were detected in either cKO or control mice (I). Data are presented as means ± SEM; $n = 3$, multiple Student's t test with Bonferroni correction. *$P < 0.05$; **$P < 0.01$; ***$P < 0.001$; ****$P < 0.0001$.

neurons (fig. S5D). Thus, SCPNs increased at the expense of deep CPNs in *CAG-CreER;Foxg1* cKO mice. We detected no differences in the proportion of TBR1^{high}BrdU^{+}/BrdU^{+} neurons between the two genotypes (fig. S5D). The increase in SCPNs was confirmed by staining with an antibody against the SCPN marker protein kinase C–γ (PKC-γ) (fig. S6A). Compared to control brains, the number of PKC-γ^{+} SCPNs in *CAG-CreER;Foxg1* cKO brains was remarkably increased (fig. S6B). We next used retrograde tracing to characterize SCPNs by injecting DiI (Dioctadecyl-3,3,3',3'-Tetramethylindocarbocyanine Perchlorate) into the medulla pyramid, where the corticospinal tracts are known to pass through (*2*, *39*), which also successfully confirmed the increase in SCPNs in *CAG-CreER;Foxg1* cKO brains (fig. S6, C and D). Together, these results demonstrate that deletion of *Foxg1* from E14.5 promotes the deep CPNs born at E13.5 to develop into SCPNs.

Corpus callosum, corticothalamic tracts, and corticospinal tracts do not form in *NEX-Cre;Foxg1* cKO brains lacking *Foxg1* at E11.5

The observed loss of CPN identity and arrested CFuN specification resulting from *Foxg1* disruption from E11.5 would be expected to manifest in projection phenotypes. We conducted an extensive series of labeling experiments, which ultimately confirmed that *NEX-Cre;Foxg1* cKO brains displayed a complete loss of the corpus callosum (fig. S7A), a lack of corticothalamic axons in the dorsal thalamus (fig. S7B), and a loss of the corticospinal tracts in the pons (fig. S7C) and the medulla (fig. S7D). A previous study reported that FOXG1 can form a complex with Rp58 to regulate axon projection (*25*); it seems plausible that the projection deficits we observed here may result from the combined consequences of dysregulated axonal projection and neuron subtype specification.

CAG-CreER;Foxg1 cKO brains lacking *Foxg1* at E14.5 have thicker corticospinal tracts and a thinner callosal callosum

Corresponding to that deep CPNs developed into SCPNs upon disruption of *Foxg1* at E14.5, the *CAG-CreER;Foxg1* cKO brains displayed obviously thicker corticospinal tracts (fig. S8, A and B) and an aberrantly thin corpus callosum (fig. S8C). These mice also had many fewer corticothalamic axons in the striatum and thalamus (fig. S8, D and E), further demonstrating impaired specification of CThPNs upon disruption of *Foxg1* at E14.5.

Thus, our results demonstrate how *Foxg1* deletion at E11.5 causes the loss of both deep and superficial CPNs that is accompanied by conversion of deep CPNs into CFuNs. Moreover, disruption of normal CFuN specification precludes further developmental progression toward SCPNs or CThPNs. Loss of *Foxg1* at E14.5 caused conversion of deep CPNs to SCPNs, increased levels of TBR1 but not BCL11B in superficial CPNs, and failed BCL11B down-regulation during CThPN specification. Beyond establishing that FOXG1 activates both deep and superficial CPN identities, these results support the existence of two mechanisms through which FOXG1 regulates the specification of deep and superficial CPNs.

FOXG1 functions as an activator of *Fezf2* transcription

Previous studies have shown that the precisely controlled transcription of *Fezf2* is crucial to the proper specification of deep layer cortical projection neurons, and FEZF2 protein is known to function as an upstream regulator to promote *Bcl11b* transcription in SCPNs (*13*, *15*, *17*, *18*). During CThPN specification, the levels of both FEZF2 and BCL11B must be reduced, whereas high FEZF2 and BCL11B levels are retained in SCPNs (*16*, *39*, *40*).

We performed in situ hybridization, which showed that *Fezf2* is strongly expressed at the CP at E14.5 and E16.5 (Fig. 4, A and B). Furthermore, *Fezf2* exhibited its expected SCPN^{high}CThPN^{low} expression pattern in control cortices at P0 (Fig. 4C). Unexpectedly, and apparently inconsistent with the significant increase in BCL11B that we observed in the *NEX-Cre;Foxg1* cKO cortex, *Fezf2* expression was almost undetectable at E14.5 (Fig. 4A). In addition, although a strong reduction in the *NEX-Cre;Foxg1* cKO cortex was still evident at E16.5, the elevated *Fezf2* level at this developmental stage did indicate that some slight restoration or compensatory expression was initiated by this point in the *NEX-Cre;Foxg1* cKO brains (Fig. 4B). We detected a further restoration of *Fezf2* expression at P0; however, rather than the SCPN^{high}CThPN^{low} pattern of control mice, the *NEX-Cre;Foxg1* cKO cortex displayed a uniform *Fezf2* expression pattern in the CP (Fig. 4C). Such a uniform pattern is consistent with the failed specification of CThPNs that we initially observed (Fig. 1E). Further supporting this, the same uniform *Fezf2* expression pattern was also observed in the *CAG-CreER;Foxg1* cKO cortex at P0 (Fig. 4D).

Two putative FOXG1-binding sites at the *Fezf2* locus have been previously reported, one within the promotor and the other within a downstream enhancer (Fig. 4E) (*41*). To explore the spatiotemporal regulation of *Fezf2* transcription during SCPN and CThPN specification, we performed ChIP–quantitative polymerase chain reaction (qPCR) at E14.5 with an anti-FOXG1 antibody in the control cortex, seeking to measure FOXG1 enrichment at the two putative binding sites. The enrichment at both the promotor and enhancer sites was quite high (Fig. 4, F and G). Luciferase assays showed an obvious activation of FOXG1 at the *Fzef2* promotor, and this activation was weakened when FOXG1-binding motifs were deleted (Fig. 4, H and I). Very weak activation was observed on the enhancer site, and point mutations in FOXG1-binding motifs at the *Fezf2* enhancer did not obviously affect its activity (Fig. 4J). These results indicate that the promoter site but not the enhancer site serves as a strong direct regulatory element for FOXG1 (Fig. 4K). We next assessed *Fezf2* mRNA expression from E12.5 to P0 and detected a peak at E15.5 (Fig. 4L), a transcription trend coincident with that the FEZF2 protein was highly expressed in all CFuNs but was later down-regulated during the specification of CThPNs (Fig. 4, A to C). Collectively, these results support that FOXG1 functions as an activator of *Fezf2* transcription.

FOXG1 promotes transcription of multiple *Sox* family members

It has been reported that SOX5, a member of the SOXD (the N-terminal Sry-related HMG box subfamily D) subfamily, controls CThPN specification by down-regulating *Fezf2*, while SOX4 and SOX11 [members of the SOXC (the N-terminal Sry-related HMG box subfamily C) subfamily] are required to retain a high FEZF2 level in SCPNs (*20*–*22*). Thus, the arrested development of CFuNs that we observed in *Foxg1* cKO mice suggests the possible involvement of SOX members. We conducted immunostaining, which showed that SOX5 was strongly expressed at the CP at E14.5 in control mice, after which its expression was confined to SCPNs and CThPNs (E16.5 to P0) (Fig. 5A), consistent with the reported role of this SOXD subfamily member in SCPN and CThPN specification, little if any SOX5 was detected in the *NEX-Cre;Foxg1* cKO cortex (Fig. 5A).

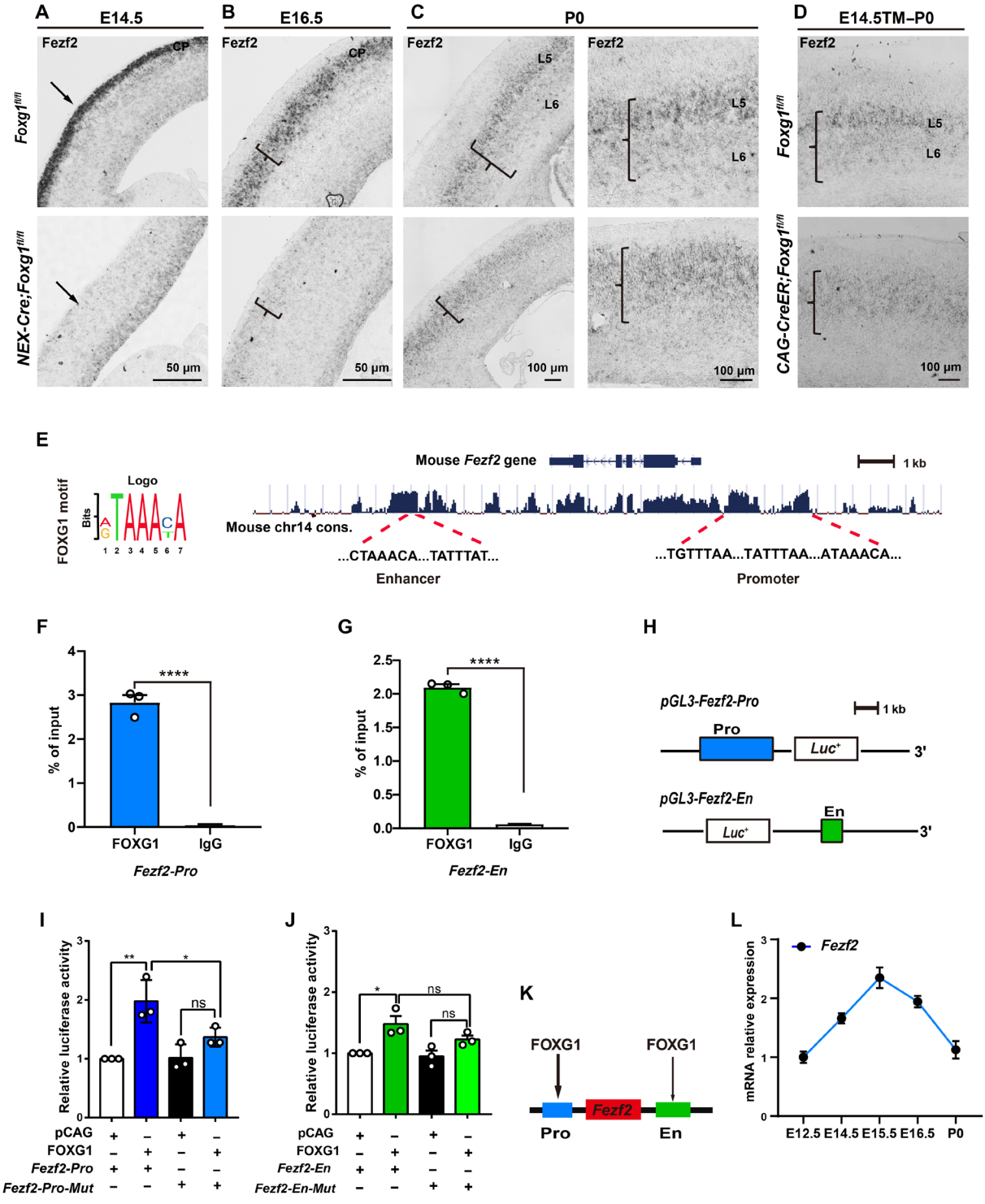

Fig. 4. FOXG1 directly promotes *Fezf2* transcription. (**A** to **D**) In situ RNA hybridization showing significantly decreased *Fezf2* mRNA level in *NEX-Cre;Foxg1* cKO CPs at E14.5 (A) and E16.5 (B). At P0, *Fezf2* mRNA expression displayed a $SCPN^{high}CThPN^{low}$ pattern in the control but a uniform expression pattern at the *NEX-Cre;Foxg1* cKO CPs (C). Similarly, *Fezf2* mRNA also displayed a uniform expression pattern in the *CAG-CreER;Foxg1* cKO cortex at P0 (D). (**E**) Motif analyses and prediction of the FOXG1-binding site(s) at the *Fezf2* locus. (**F** and **G**) ChIP-qPCR of cortex samples at E14.5, showing enriched FOXG1 occupancies at both the promoter and enhancer sites of the *Fezf2* locus. (**H**) Strategy for constructing the vector for the *Fezf2* promoter and enhancer for luciferase assays. (**I** and **J**) Luciferase assay showing the activation of FOXG1 at the *Fezf2* promoter site (I), while showing very weak activation at the *Fezf2* enhancer site (J). Deletion of the FOXG1-binding motifs from the *Fezf2* promoter reduced the extent of FOXG1-mediated activation of the luciferase reporter. (**K**) Summary model for FOXG1's regulation of *Fezf2* expression via binding at the *Fezf2* promoter and/or enhancer sites. (**L**) qPCR of cortex samples to monitor *Fezf2* mRNA levels over the course of cortical development from E12.5 to P0. Data are presented as means ± SEM; (F and G) unpaired Student's *t* test and (I and J) one-way analysis of variance (ANOVA) followed by Tukey-Kramer post hoc test. $^{*}P < 0.05$, $^{**}P < 0.01$; $^{****}P < 0.0001$.

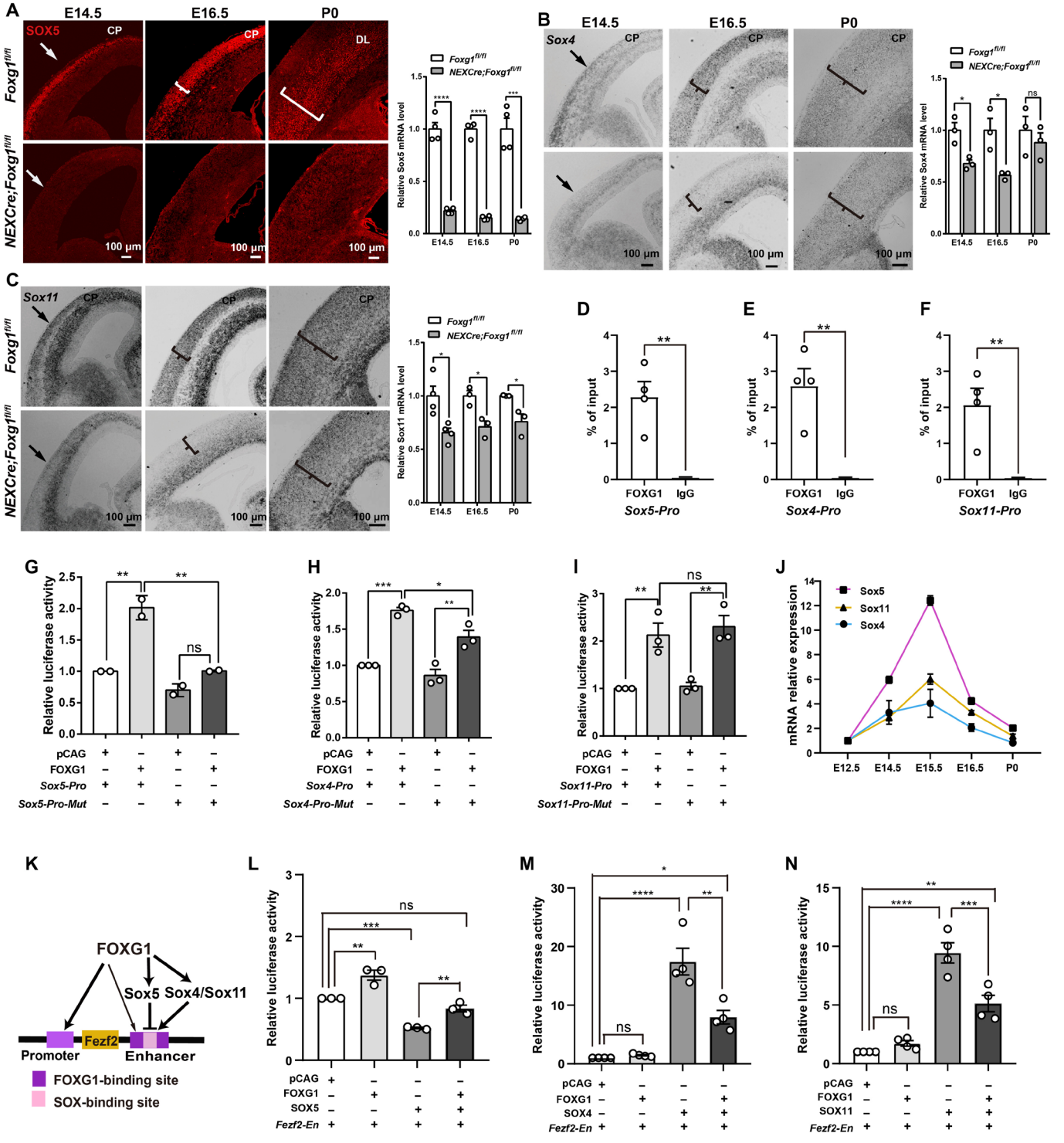

Fig. 5. FOXG1 promotes the transcription of *Sox* members and coordinates SOXs to precisely control the level of FEZF2. (**A**) Immunostaining and qPCR showing significantly decreased SOX5 in *NEX-Cre;Foxg1* cKO compared with the control mice during E14.5 to P0. (**B** and **C**) In situ hybridization and qPCR showing that *Sox4* (B) and *Sox11* (C) were markedly decreased at E14.5 and E16.5 but were elevated at P0 in the *NEX-Cre;Foxg1* cKO mice. (**D** to **F**) ChIP-qPCR of cortex samples from E14.5, showing strong enrichment of FOXG1 at promoter sites of *Sox5*, *Sox4*, and *Sox11* loci. (**G** to **I**) Luciferase assay showing the activation of FOXG1 on *Sox5* (G), *Sox4* (H), and *Sox11* (I). Point mutations in FOXG1-binding motifs in the *Sox5* promoter and deletion of the FOXG1-binding motifs from the *Sox4* promoter caused reduced reporter activation (G and H); no reduction was detected upon its deletion from the *Sox11* promoter (I). (**J**) qPCR analysis showing mRNA levels of *Sox* members. (**K**) Exploratory model about FOXG1's regulation of *Fezf2* transcription mediated via binding competition with SOX proteins. The thin arrow indicates the weak activation of FOXG1 at the *Fezf2* enhancer site. (**L** to **N**) Luciferase assay showing the competition between FOXG1 and SOX members. Data were presented as means ± SEM; (D to F) unpaired Student's *t* test and (G to I and L to N) one-way ANOVA followed by Tukey-Kramer post hoc test. **P* < 0.05; ***P* < 0.01; ****P* < 0.001; *****P* < 0.0001.

Furthermore, in situ hybridization experiments showed that the SOXC subfamily members *Sox4* and *Sox11* were strongly expressed in control postmitotic neurons at the CP during E14.5 to P0 (Fig. 5, B and C). In contrast, the *NEX-Cre;Foxg1* cKO mice displayed remarkably decreased *Sox4* and *Sox11* expression levels, specifically in postmitotic neurons from which *Foxg1* was deleted (Fig. 5, B and C). It bears emphasis that both SOX4 and SOX11 levels were somewhat restored at the CP at P0 compared with the E14.5 to E16.5 levels (Fig. 5, B and C). Thus, the expression trends we observed for SOXC subfamily members are temporally consistent with the reported function of these proteins in maintaining FEZF2 levels in SCPN and CThPN specification and with our observations of FEZF2 levels in the *NEX-Cre;Foxg1* cKO cortex (Fig. 4, A to C).

We next examined whether FOXG1 directly transcriptionally activates *Sox* family genes. A bioinformatics analysis using the UCSC Genome Browser indicated apparent conservation of putative FOXG1-binding sequences (*42*) in the promoter regions of *Sox* family members. We conducted ChIP-qPCR and found that FOXG1 was highly enriched at the promoter regions of *Sox5*, *Sox4*, and *Sox11* in the E14.5 control cortex (Fig. 5, D to F). Luciferase assays showed obvious activations of FOXG1 at the *Sox4*, *Sox5*, and *Sox11* promotors (Fig. 5, G to I). Deletion of FOXG1-binding motifs from the *Sox4* promotor and point mutations at the *Sox5* promotor weakened the activations of FOXG1 (Fig. 5, G and H). However, the luciferase activity was not obviously changed when FOXG1-binding motifs were deleted from the *Sox11* promotor (Fig. 5I), suggesting that FOXG1 regulates *Sox11* transcription through coordinating with some as-yet-unknown partner. qPCR analysis of whole control cortex samples showed that mRNA expression levels for these three *Sox* members were gradually increased from E12.5 onward, reaching a peak around E15.5 (Fig. 5J). These results establish that FOXG1 directly binds to the promoters of *Sox5* and *Sox4* and positively regulates their transcription, while activation of *Sox11* apparently involves other regulatory mechanisms.

The proper *Fezf2* dosage required to specify SCPN versus CThPN fate is precisely controlled through FOXG1 and SOX competition

Previous studies have demonstrated that SOX5 and SOX4/SOX11 competitively bind to an enhancer at the *Fezf2* locus: This leads not only to FEZF2 down-regulation in CThPNs but also to maintenance of high FEZF2 levels in SCPNs during specification (*20*). It was therefore highly conspicuous when we found that the SOX-binding motif at the *Fezf2* locus was embedded within multiple FOXG1-binding motifs present in the same enhancer domain (Fig. 5K). This finding strongly suggested the possibility that FOXG1 may compete with SOX members to control the precise expression of FEZF2. Pursuing this hypothesis, we generated overexpression vectors for *Sox5*, *Sox4*, and *Sox11*. Subsequent luciferase reporter assays with these *Sox* vectors and the *Fezf2*-En vector revealed that transfection with *Sox5* led to a 47.9 ± 1.2% decrease in reporter activity, consistent with SOX5 as a repressor of *Fezf2* transcription. Simultaneous transfection with the reporter vector alongside both the *pCAG-Foxg1* and *pCAG-Sox5* vectors significantly increased reporter activity compared with the *Sox5* vector alone (0.84 ± 0.03 versus 0.52 ± 0.01), indicating that competitive binding of FOXG1 at the enhancer element of the *Fezf2* locus can alleviate SOX5-mediated repression of *Fezf2* transcription (Fig. 5L).

Conversely, transfection with the *Sox4* or *Sox11* vectors resulted in 17- and 9-fold increases in reporter activity (compared with cells harboring the reporter vector alone), findings demonstrating the strong *Fezf2* transcriptional activation function of these SOXC subfamily proteins (Fig. 5, M and N). We found that simultaneous transfection of the *Foxg1* vector with the *Sox4* or *Sox11* vectors reduced reporter activity significantly (only eight- and fourfold over the reporter vector alone cells) (Fig. 5, M and N). Thus, these results are, on the one hand, consistent with the idea of competitive FOXG1 versus (general) SOX protein binding at the *Fezf2* enhancer. On the other hand, these results also indicate that the strength of FOXG1's transcriptional activation impacts—specifically at the enhancer region of *Fezf2*—is substantially weaker than the induction effects of *Sox4* and *Sox11*. These results, when viewed alongside our earlier findings about the much stronger activation from the promoter-localized FOXG1-binding site relative to the enhancer-localized FOXG1-binding site, unveil a complex regulatory network for controlling *Fezf2* expression to specify CThPN and SCPN fate.

FOXG1 directly activates *Satb2* and represses both *Tbr1* and *Bcl11b*

Considering the significant reduction of SATB2 we observed in both deep and superficial CPNs in both *NEX-Cre;Foxg1* cKO and *CAG-CreER;Foxg1* cKO mice (Figs. 1, C to E, and 2, D and E), we analyze the sequence of the *Satb2* locus and identified a putative consensus FOXG1-binding site within the promoter (Fig. 6A). We next performed ChIP-qPCR and detected a strong FOXG1 enrichment in the E14.5 control cortex (Fig. 6B). Luciferase assays demonstrated that FOXG1 can directly activate *Satb2*, and deletion of binding motifs weakened the activation (Fig. 6C). qPCR analysis revealed a continuous increase in *Satb2* mRNA expression during E12.5 to P0 (Fig. 6D), the developmental window when a majority of CPNs are produced and specified (*5*). Thus, FOXG1 acts as an activator of *Satb2*.

It is reported that during the acquisition of superficial competence, FOXG1 may derepress *Fezf2* through repressing *Tbr1* (*43*). In the present study, *Tbr1* was up-regulated in both deep and superficial CPNs in *NEX-Cre;Foxg1* cKO and *CAG-CreER;Foxg1* cKO mice. ChIP-qPCR revealed strong FOXG1 occupancy at the *Tbr1* promoter at E14.5 (Fig. 6, E and F). Luciferase assays revealed that FOXG1 functions as a direct repressor of *Tbr1* transcription, and deletion of FOXG1-binding motifs weakened the repression on the *Tbr1* promotor (Fig. 6G). qPCR analysis showed that *Tbr1* mRNA level was high during E12.5 to E14.5 but decreased afterward (Fig. 6H). These results support that FOXG1 may directly inhibit *Tbr1* transcription in both deep and superficial CPNs.

Although BCL11B has been reported as a downstream target of FEZF2 signaling (*13*), disruption of *Fezf2* resulted in loss of BCL11B. However, ectopic expression of *Fezf2* by in utero electroporation was unable to induce BCL11B expression (*13*), suggesting that *Bcl11b* is also controlled via an as-yet-unknown FEZF2-independent pathway. To date, there is no evidence confirming that FEZF2 can directly influence BCL11B accumulation. We also found that BCL11B is massively up-regulated in CThPNs and deep CPNs at P0 in *CAG-CreER;Foxg1* cKO mice; recall that these mice have severely decreased FEZF2 levels, again suggesting that *Bcl11b* may be controlled via an unknown FEZF2-independent pathway.

Pursuing this FEZF2-independent speculation, we identified multiple putative FOXG1-binding motifs within a distal 50-kb

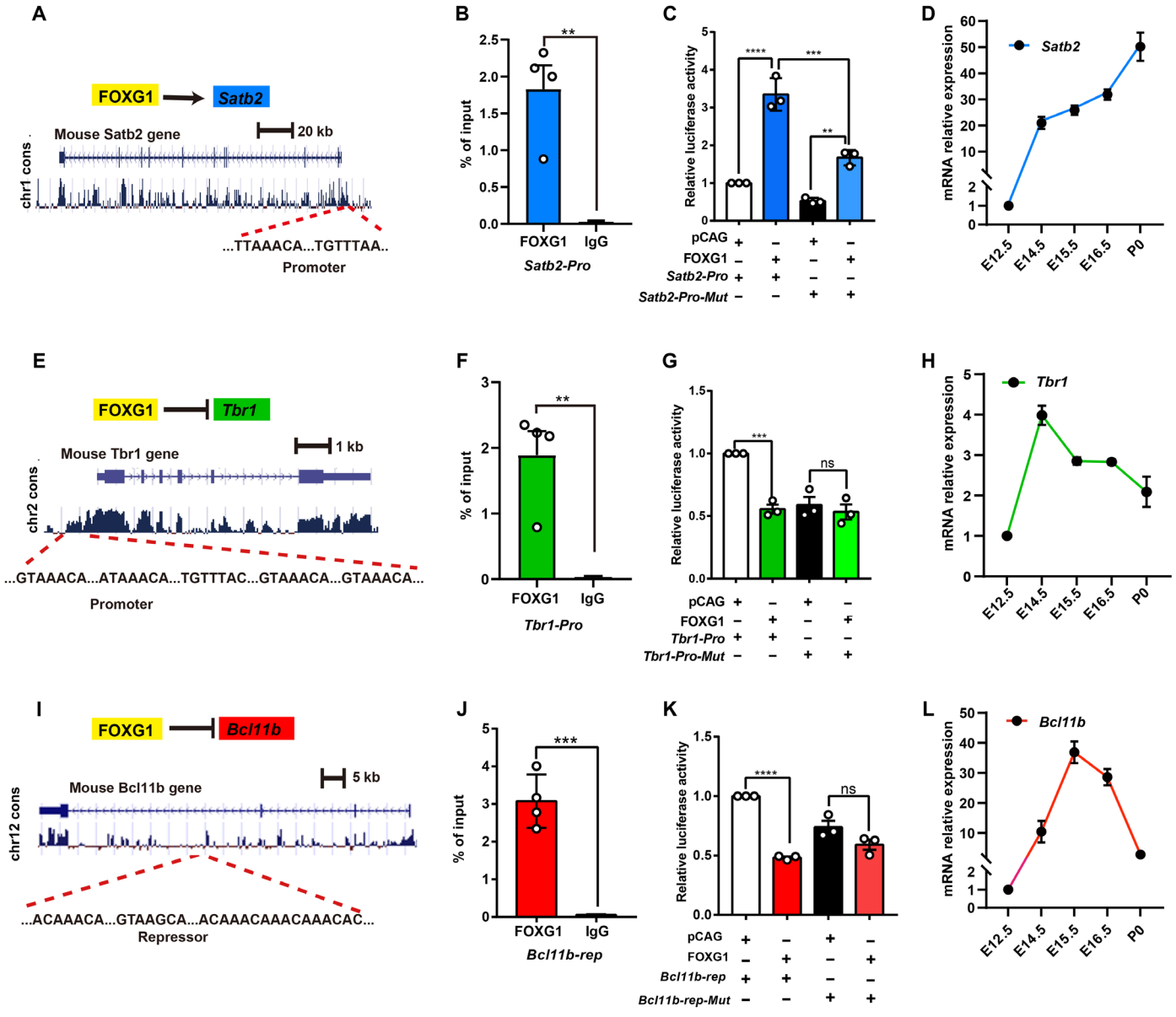

Fig. 6. FOXG1 directly promotes *Satb2* but suppresses *Tbr1* and *Bcl11b*. (**A**) Motif analyses and prediction of FOXG1-binding site at *Satb2* locus. (**B**) ChIP-qPCR with cortex samples from E14.5, showing high FOXG1 occupancy at the promotor site of the *Satb2*. (**C**) Luciferase assay showing that FOXG1 directly activates *Satb2* by binding at the promoter site, and deletion of FOXG1-binding motifs from *Satb2* promoter weakened its activation. (**D**) qPCR with cortex sample–assessed *Satb2* mRNA from E12.5 to P0. (**E**) Motif analyses and prediction of FOXG1-binding site at *Tbr1* locus. (**F**) ChIP-qPCR with cortex samples from E14.5, showing high FOXG1 occupancy at the promotor site of the *Tbr1*. (**G**) Luciferase assay showing that FOXG1 directly represses *Tbr1* transcription by binding at the promoter site; deletion of FOXG1-binding motifs from the *Tbr1* promoter weakened the extent of FOXG1's repression of transcription. (**H**) qPCR with cortex sample–assessed *Tbr1* mRNA from E12.5 to P0. (**I**) Motif analyses and prediction of FOXG1-binding site at *Bcl11b* locus. (**J**) ChIP-qPCR with cortex samples from E14.5, showing high FOXG1 occupancy at the repressor site of *Bcl11b*. (**K**) Luciferase assay showing that FOXG1 directly represses *Bcl11b* transcription by binding at the repressor site; deletion of FOXG1-binding motifs from *Bcl11b* repressor element weakened its repression. (**L**) qPCR with cortex sample–assessed *Bcl11b* mRNA from E12.5 to P0. Data were presented as means ± SEM; (B, F, and J) unpaired Student's *t* test and (C, G, and K) one-way ANOVA followed by Tukey-Kramer post hoc test. $^{**}P < 0.01$; $^{***}P < 0.001$; $^{****}P < 0.0001$.

conserved region of the *Bcl11b* locus (Fig. 6I). ChIP-qPCR analysis revealed a high enrichment in the binding site (Fig. 6J). Luciferase assays showed that FOXG1 negatively regulates *Bcl11b* transcription by binding to the distal repressor site (Fig. 6K). qPCR showed that the *Bcl11b* mRNA level reached a peak at E15.5 and then rapidly declined (Fig. 6L). These results demonstrate that FOXG1 strongly represses *Bcl11b* transcription.

Cell type–specific disruptions/overexpression establish that FOXG1 controls cortical neuron subtype–specific gene expression programs

To experimentally confirm FOXG1's repression of *Bcl11b* in CThPNs, we used *Ntsr1-Cre* mice (*44*)—which enable specific cKO of *Foxg1* in CThPNs after E14.5—to detect the effects of *Foxg1* deletion on CThPN specification. At P8 when the specification

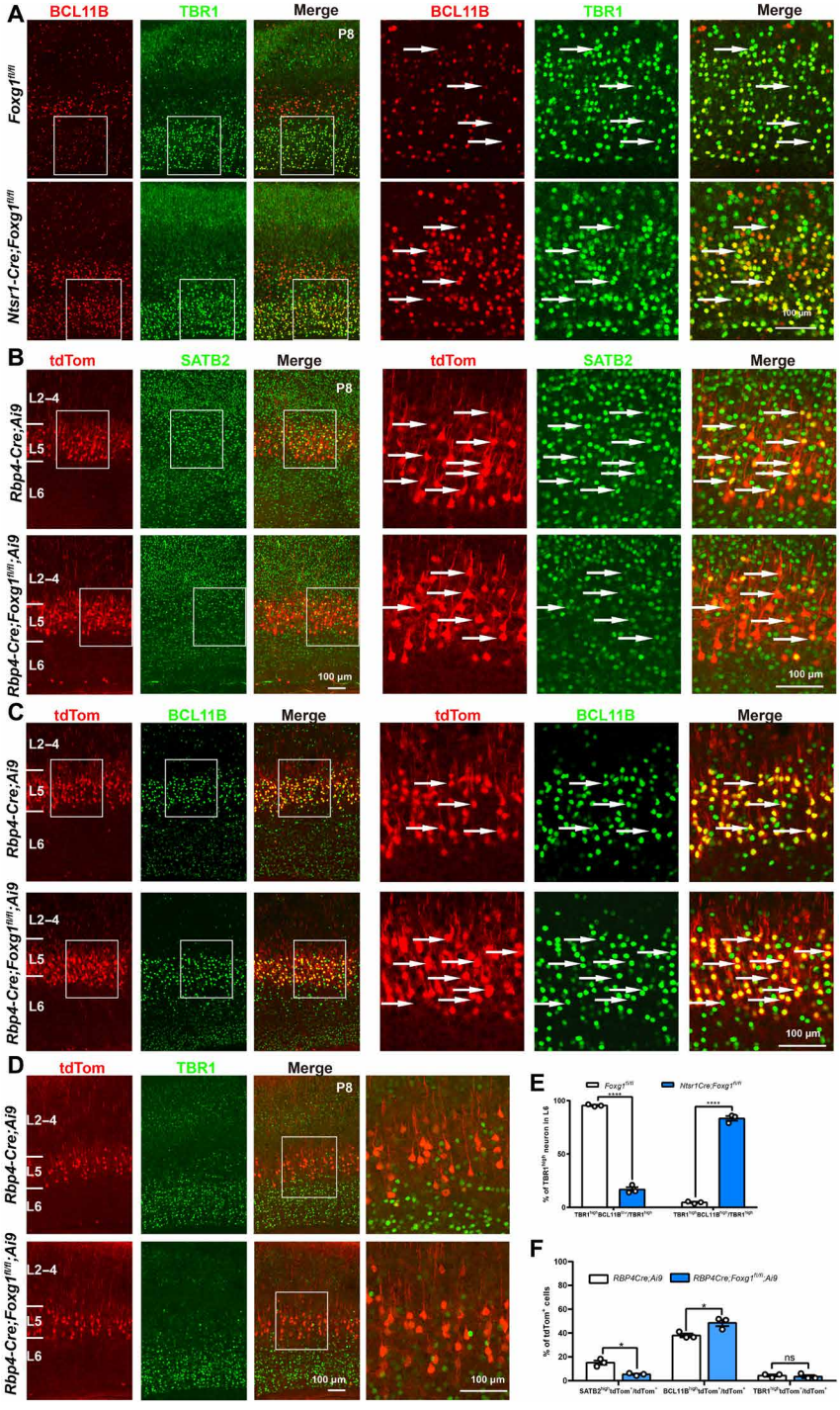

Fig. 7. Cell type–specific disruption further demonstrated that FOXG1 controls subtype-specific gene expression programs. (**A**) Double immunostaining against TBR1 and BCL11B at P8. Control mice have low BCL11B levels in CThPNs. *Ntsr1-Cre;Foxg1* cKO mice feature CThPN-specific disruption of *Foxg1*, and these cells had high BCL11B levels. (**B**) Double immunostaining against tdTom and SATB2 at P8. *Rbp4-Cre;Ai9;Foxg1* cKO mice feature disruption of *Foxg1* from both deep CPNs and SCPNs, which are labeled by tdTom. Compared with control mice, SATB2^{high}tdTom^{+} deep CPNs remarkably reduced in *Rbp4-Cre;Ai9;Foxg1* cKO mice. (**C**) Double immunostaining against tdTom and BCL11B at P8, showing that BCL11B^{high}tdTom^{+} SCPNs increased in *Rbp4-Cre;Ai9;Foxg1* cKO mice. (**D**) Double immunostaining against tdTom and TBR1 at P8. There was no difference in TBR1 levels in tdTom^{+} neurons in *Rbp4-Cre;Ai9* or *Rbp4-Cre;Ai9;Foxg1* cKO animals, a finding indicating that FOXG1 does not affect TBR1 expression in deep CPNs or SCPNs. (**E**) Quantitative analysis of neurons in L6, showing the decreased percentages of TBR1^{high}BCL11B^{low} neurons in TBR1^{high} neurons and the increased percentage of TBR1^{high}BCL11B^{high} neurons in *Ntsr1-Cre;Foxg1* cKO mice at P8. (**F**). Quantitative analysis of neurons in L5, showing the decreased percentages of SATB2^{high}tdTom^{+} neurons in tdTom^{+} neurons and the increased percentage of BCL11B^{high}tdTom^{+} neurons in *Rbp4-Cre;Foxg1* cKO mice at P8. Few TBR1^{high}tdTom^{+} neurons were observed in both control and *Rbp4-Cre;Foxg1* cKO mice, and no obvious changes were detected in *Rbp4-Cre;Foxg1* cKO mice. Data are presented as means ± SEM; $n = 3$, multiple Student's *t* test with Bonferroni correction. *$P < 0.05$; ****$P < 0.0001$.

of cortical projection neuron subtypes is finished, we detected failed down-regulation of BCL11B in *Ntsr1-Cre;Foxg1* cKO CThPNs (Fig. 7, A and E).

We next examined *Rbp4-Cre;Ai9;Foxg1* cKO mice—in which *Foxg1* is specifically knocked out after E14.5 in deep CPNs and SCPNs, which are both labeled by a tdTomato reporter—seeking to experimentally confirm two FOXG1 functions after E14.5: (i) that FOXG1 activates *Satb2* but represses *Bcl11b* in deep CPNs and (ii) that FOXG1 has no impact on the *Tbr1* in deep CPNs and SCPNs. At P8, many tdTom$^+$ neurons in the control mice were SATB2$^+$, while the number of SATB2$^+$tdTom$^+$ was significantly decreased in *Rbp4-Cre;Ai9;Foxg1* cKO mice (Fig. 7B). Meanwhile, a large number of the tdTom$^+$ neurons in the *Rbp4-Cre;Ai9;Foxg1* cKO mice were BCL11B^{high} (Fig. 7C). Quantification analysis showed that the percentage of SATB2$^+$tdTom$^+$ deep CPNs among tdTom$^+$ neurons was obviously decreased in *Rbp4-Cre;Ai9;Foxg1* cKO mice compared with that of control mice, while the percentage of BCL11B$^+$tdTom$^+$ SCPNs among tdTom$^+$ neurons was increased (Fig. 7F). We did not detect obvious changes in TBR1 expression in tdTom$^+$ neurons between the control and *Rbp4-Cre;Ai9;Foxg1* cKO mice (Fig. 7, D and F). Together, these results confirm that lacking *Foxg1* causes deep CPNs to develop into SCPNs and show that FOXG1 activates *Satb2* but represses *Bcl11b* in deep CPNs. Note that no aberrant accumulation of TBR1 was observed in tdTom$^+$ neurons of *Rbp4-Cre;Ai9;Foxg1* cKO mice (Fig. 7, D and F), further supporting our conclusion that FOXG1 does not repress *Tbr1* in deep CPNs or SCPNs after E14.5.

To further examine the role of FOXG1 in controlling the specification of CFuNs versus deep CPNs, we overexpressed *Foxg1* by crossing *NEX-Cre* with a *CAG-loxp-stop-loxp-Foxg1-IRES-EGFP* mouse line (fig. S9, A and E) (*45*): We found an obvious increase in the SATB2 level in both BCL11B$^+$ SCPNs and TBR1$^+$ CThPNs, in which *Foxg1* was overexpressed when measured on the basis of fluorescence intensity (fig. S9, B, E, and F). We found that the BCL11B level was slightly decreased in *Foxg1*-overexpressing SCPNs; no obvious changes were detected in the TBR1 level in *Foxg1*-overexpressing CThPNs (fig. S9, C to F). Because we did not detect obvious accumulation of BCL11B in *Foxg1*-deficient SCPNs and considering that SATB2 is demonstrated to directly repress *Bcl11b* (*14*, *36*), here the decreased level of BCL11B might be caused by the increased SATB2 level in *Foxg1*-overexpressing SCPNs. Together, our results show that FOXG1 is capable for the induction of *Satb2* in both CThPNs and SCPNs but is insufficient for the repression of (i) *Tbr1* in CThPNs and (ii) *Bcl11b* in SCPNs.

To experimentally further confirm that (i) FOXG1 activates *Satb2* in both developing deep and superficial CPNs, (ii) FOXG1 represses *Tbr1* in superficial CPNs, and (iii) FOXG1 represses *Bcl11b* in deep CPNs, we used a *Satb2-Cre-IRSE-GFP* line in which *GFP* cDNA was introduced into *Satb2* locus (*46*) to delete *Foxg1* in CPNs. We first examined the expression pattern of GFP during the time window of E13.5 to E18.5 and found that GFP exhibited the same expression pattern as SATB2 in *Satb2-Cre-IRSE-GFP* mice, thereby confirming that GFP$^+$ neurons represent both SATB2$^+$ deep CPNs and superficial CPNs (Fig. 8, A to C).

We then explored the efficiency of *Foxg1* deletion and the identities of *Foxg1*-deficient neurons in *Satb2-Cre-GFP;Foxg1* cKO brains. At E13.5, a time point when very few of deep CPNs appeared in the CP, we found the FOXG1 level was not obviously changed in GFP$^+$ neurons in the CP in *Satb2-Cre-GFP;Foxg1* cKO mice, suggesting that *Foxg1* was not obviously disrupted at E13.5 in the developing cortex. No obvious change in the SATB2 level was detected at this time point either (Fig. 8A).

At E16.5, we found the expression level of FOXG1 was significantly decreased in the majority of GFP$^+$ neurons in *Satb2-Cre-GFP;Foxg1* cKO cortices (Fig. 8B). Note that expression of GFP was also severely decreased. Because *GFP* was introduced into the *Satb2* locus in the *Satb2-Cre-GFP* line, GFP expression is likely to be regulated by the activation of FOXG1 on the *Satb2* promotor as well, which could result in this observed decrease in GFP. It seemed that *Foxg1* was not disrupted in a small number of CPNs in which high levels of FOXG1, GFP, and SATB2 remained (Fig. 8B). Similar results were obtained at E18.5 in *Satb2-Cre-GFP;Foxg1* cKO mice (Fig. 8C). We then examined the identities of GFP^{weak}FOXG1^{weak} neurons at E18.5. The expression level of SATB2 was significantly decreased throughout *Satb2-Cre-GFP;Foxg1* cKO cortices (Fig. 8C), and this was accompanied by an obvious accumulation of BCl11B in the deep layer and a slight increase in TBR1 in the superficial layer (Fig. 8, D and E). Quantification of fluorescence intensity showed that TBR1 level was increased in GFP^{weak}FOXG1^{weak} neurons, which populated in the superficial layer (Fig. 8G), similar to the observations in *CAG-Cre;Foxg1* cKO mice. In GFP^{weak}FOXG1^{weak} neurons in the deep layer, BCl11B was significantly increased (Fig. 8F). Together, these results reveal that FOXG1 activates *Satb2* in both deep and superficial CPNs, represses *Tbr1* in superficial CPNs, and represses *Bcl11b* in deep CPNs. Collectively, these various cell type–specific disruption and overexpression experiments establish that FOXG1 controls postmitotic projection neuron subtype specification in both developmental stage–specific and neuron subtype–specific manners, doing so by regulating both induction and repression programs (Fig. 9).

DISCUSSION

Much remains unknown about the sequential postmitotic specification of neuron subtypes during cortical development. By combining cKO mice and finely time-resolved sampling, we here show that the transcription factor FOXG1 exerts at least four major regulatory impacts during cortical neuron development. First, in postmitotic neurons before E14.5, FOXG1 directly activates *Satb2* and represses both *Bcl11b* and *Tbr1* to enforce deep CPN identity. Second, for specification of superficial CPNs and deep CPNs (after E14.5), FOXG1 still activates *Satb2* and represses *Tbr1* but no longer represses *Bcl11b* in superficial CPNs. Conversely, FOXG1 no longer represses *Tbr1* in deep CPNs. Third, we found a sophisticated regulatory axis wherein FOXG1 specifies CThPN versus SCPN fate after E14.5 by fine-tuning *Fezf2* levels: FOXG1 directly activates transcription of both *Fezf2* and multiple *Sox* family genes (*Sox5* and *Sox4/Sox11*); FOXG1 then competes with SOX proteins for binding at an enhancer site in the regulatory region of the *Fezf2* locus. Fourth, we finally show that FOXG1 also directly represses *Bcl11b* transcription in CThPNs from E14.5 onward (Fig. 9).

Among the forkhead transcription factor family, FOXG1 represents a single subclass and consists of a proline-rich transcriptional activation domain (N-terminal) (*47*–*49*), a forkhead DNA binding domain, a Groucho-binding domain to recruit Groucho/TLE (Transducin-like Enhancer of Split-1) forming a transcriptional corepressor complex, and a JARID1B (the H3K4me2/3 histone demethylase Jarid1b)–binding domain (through which FOXG1

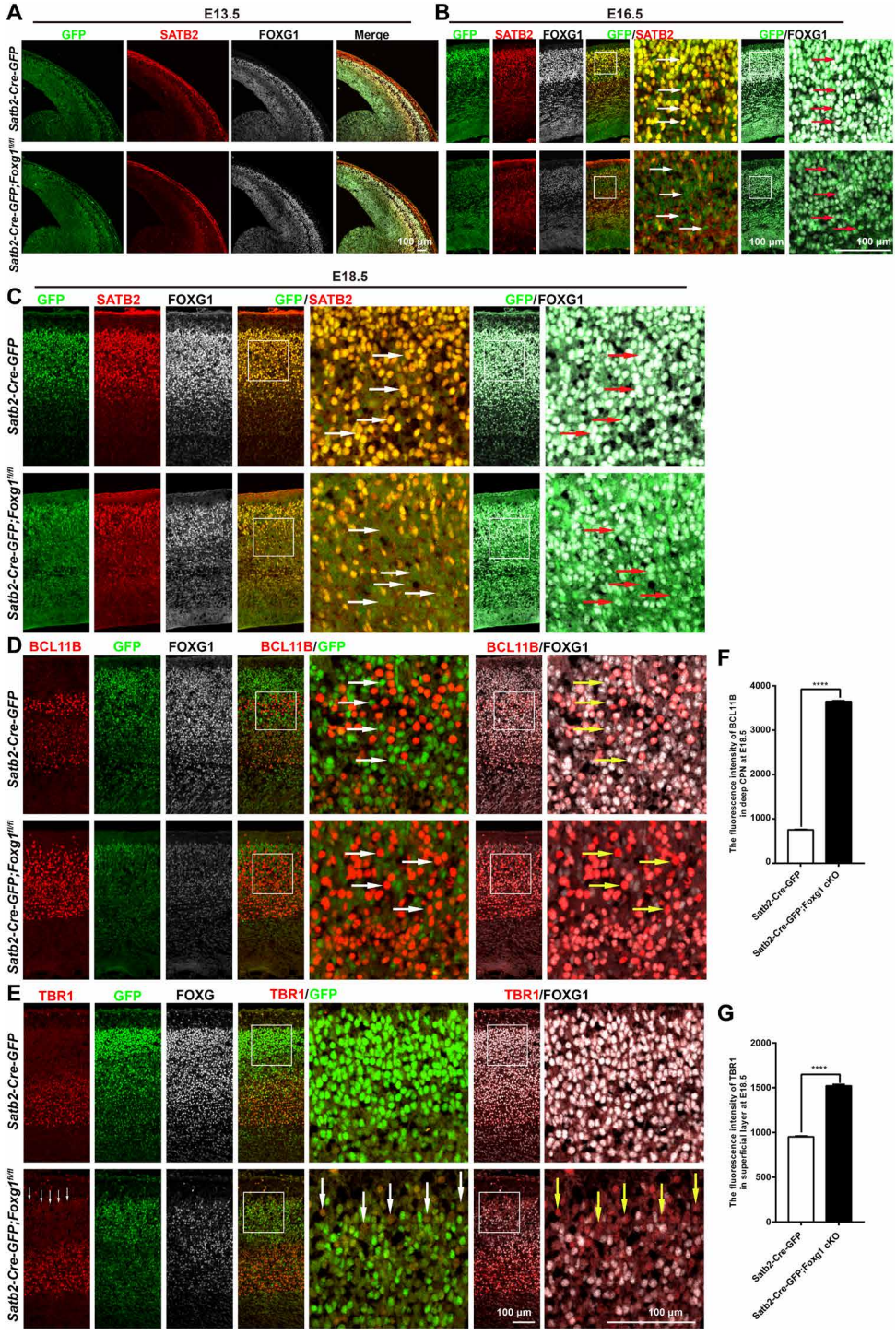

Fig. 8. Disruption of *Foxg1* in CPNs. (**A**) Triple immunostaining for GFP, SATB2, and FOXG1 at the E13.5 cortex, showing that very few GFP^{+}SATB2^{+} CPNs existed in the CP in both control and *Satb2-Cre-GFP;Foxg1* cKO mice. The level of FOXG1 was comparable between control and *Satb2-Cre-GFP;Foxg1* cKO mice. SATB2 level was also comparable. (**B** and **C**) Triple immunostaining for GFP, SATB2, and FOXG1 at the E16.5 and E18.5 cortices, showing that GFP was strongly coexpressed in both of SATB2^{+} deep CPNs and superficial CPNs (arrows) in control mice. In *Satb2-Cre-GFP;Foxg1* cKO mice, the levels of both FOXG1 and GFP were significantly decreased, and SATB2 was also severely reduced in GFP^{weak}FOXG1^{weak} neurons (arrows). (**D**) Triple immunostaining for GFP, BCL11B, and FOXG1 at the E18.5 cortex. BCL11B was not expressed in many GFP^{strong}FOXG1^{strong} deep CPNs in the control mice (arrows). In the *Satb2-Cre-GFP;Foxg1* cKO mice, BCl11B significantly accumulated in GFP^{weak}FOXG1^{weak} neurons in the deep layer (arrows). (**E**) Triple immunostaining for GFP, TBR1, and FOXG1 at the E18.5 cortex, showing a slight increase in TBR1 in GFP^{weak}FOXG1^{weak} neurons in the superficial layer in the *Satb2-Cre-GFP;Foxg1* cKO mice (arrows). (**F**) Quantification of fluorescence intensity, showing that BCl11B was significantly increased in GFP^{weak}FOXG1^{weak} neurons of the deep layer in the *Satb2-Cre-GFP;Foxg1* cKO mice. (**G**) Quantification of fluorescence intensity, showing that TBR1 level was increased in GFP^{weak}FOXG1^{weak} neurons, which populated in the superficial layer. Data were presented as means ± SEM; unpaired Student's *t* test. ****$P < 0.0001$.

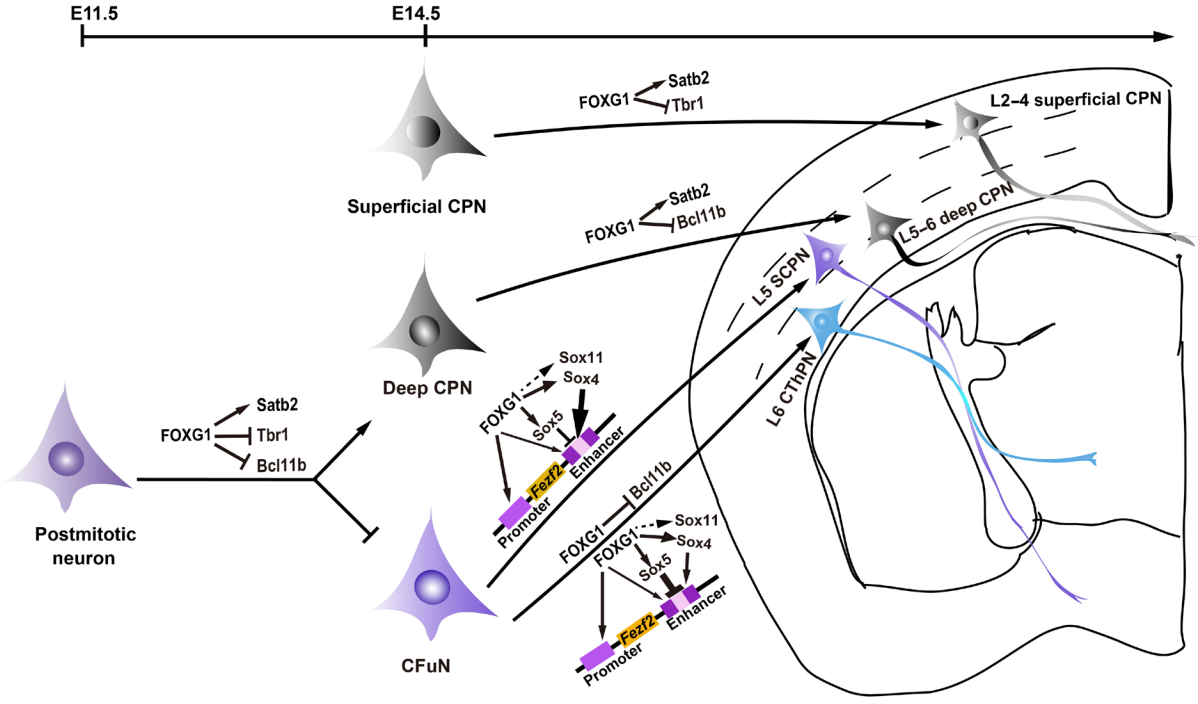

Fig. 9. Summary model of the multiple regulatory functions of FOXG1 in spatiotemporally controlling postmitotic specification of cortical projection neurons. "⊣" indicates the dominant repression of SOX5 on *Fezf2*. The thick arrow indicates the dominant activation of SOX4/SOX11 on *Fezf2*. The thin arrow indicates the weak activation of FOXG1 at the *Fezf2* enhancer site.

epigenetically represses its garget genes) (*50*–*52*). In recent years, numerous studies have demonstrated pleiotropic roles of FOXG1, ranging from cell proliferation and migration to cortical circuit specialization during telencephalon development (*25*, *53*–*55*). FOXG1 exerts multiple functions, including both repression and activation roles, based on forming a complex with specific proteins crucial for gene expression or by directly binding to cis-regulatory elements of its target genes. For instance, it has been reported that FOXG1 (i) represses *Coup-TFI* by binding at its repressor (*56*), (ii) represses *Wnt8b* by binding to its promotor (*57*), and (iii) represses *Robo1*, *Slit3*, and *Reelin* by forming a FOXG1-RP58 complex that directly binds at *Foxg1-Rp58*–binding sites (*25*). It has also been demonstrated that FOXG1 activates *Kcnh3* by binding at its enhancer (*58*). FOXG1 may directly activate *Fgf8* (*59*) and *Sox9 (60)*. Thus, FOXG1 variously controls both induction and repression programs, doing so in both developmental stage–specific and neuron subtype–specific manners.

Fate choice of deep CPNs versus CFuNs before E14.5

Deep CPNs share a common birthdate with CFuNs during early corticogenesis. These newborn neurons proceed along two distinct trajectories: toward TBR1^{high}BCL11B^{high}SATB2^{-} CFuNs or toward TBR1^{low}BCL11B^{low}SATB2^{high} deep CPNs (*8*). It is known that the *Satb2* transcription must be postmitotically activated and that *Bcl11b* and *Tbr1* have to be repressed to enforce deep CPN identity (*14*, *36*, *61*). We are unaware of any postmitotic studies that have specifically investigated how deep CPN versus CFuN identity is specified before E14.5. We have data starting from E11.5, and we show that *Foxg1* disruption in postmitotic neurons causes deep CPNs to develop into CFuNs. Specifically, these results support that FOXG1 specifies deep CPN identity by directly activating *Satb2* and simultaneously repressing both *Bcl11b* and *Tbr1* in these cells.

There is an apparent discrepancy between our detection of elevated BCL11B and a report of decreased BCL11B in the CP in *NEX-Cre;Foxg1* cKO mice (*25*). Some methodological considerations bear mention. Our findings about elevated BCL11B were based on quantification of the number of BCL11B^{+} neurons, as well as on cell tracing using BrdU. The conclusion from Cargnin *et al.* (*25*) was based on an immunostaining image. Moreover, their observation that BCL11B^{+} deep layer neurons were broadly dispersed throughout the cortex is entirely in line with our findings.

It is known that CFuN specification requires postmitotic activation of *Bcl11b* and *Tbr1* (*8*, *12*). Moreover, *Fezf2* is strongly coexpressed in TBR1^{high}BCL11B^{high} CFuNs, and a *Fezf2-Bcl11b* pathway has been reported to regulate the fate choice of SCPNs versus CPNs (*13*, *15*, *17*). Several observations from our present study are quite informative when considered in light of this background knowledge. For example, our data suggest that FEZF2 may not be required for the postmitotic maintenance of TBR1^{high}BCL11B^{high} CFuN identity, at least before E14.5: When *Foxg1* was deleted in postmitotic neurons at E11.5 in the brains of our *NEX-Cre;Foxg1* cKO mice, FEZF2 was undetectable in TBR1^{high}BCL11B^{high} CFuNs before E14.5, although cells staining for this TBR1^{high}BCL11B^{high} CFuN identity were present throughout the cortex (Fig. 4A).

FOXG1 participates in fine-scale regulation of *Fezf2* transcription in CThPNs and SCPNs via both transcriptional and protein-level engagement with SOX members

Previous work has established that SCPNs and CThPNs share a common TBR1^{high}FEZF2^{high}BCL11B^{high} molecular profile during

early corticogenesis; these cells later diverge and develop into TBR1^{high}FEZF2^{low}BCL11B^{low} CThPNs or TBR1^{low}FEZF2^{high}BCL11B^{high} SCPNs. We know that a high FEZF2 level directs CFuNs toward a SCPN fate, whereas a low level of this protein permits a CThPN fate (*15*–*18*, *39*, *62*). It was conspicuous we did not observe the expected FEZF2^{high} SCPN/FEZF2^{low} CThPN expression pattern in our cKO cortices; rather, we found that FEZF2 was expressed uniformly in both neuron subtypes, which consequently were unable to reduce the BCL11B level in CThPNs.

Here, we characterized three regulatory layers through which FOXG1 precisely regulates the extent of FEZF2 transcription. FOXG1 directly activates *Fezf2* transcription. It also activates *Sox5*, *Sox4*, and *Sox11*, three genes known to function as upstream regulators of FEZF2 transcription. Last, we show that FOXG1 can compete with SOX proteins at the *Fezf2* enhancer site. This apparently three-layer regulation of FOXG1 for *Fezf2* underscores that developing neurons are apparently highly sensitive to the FEZF2 level, which must be very precisely regulated. Previous studies have demonstrated that SOX5 exerts a dominant repression influence on *Fezf2* transcription in CThPNs, whereas SOX4/SOX11 drives overwhelming *Fezf2* activation in SCPNs (*20*–*22*). Note that FEZF2 expression was severely reduced in *NEX-Cre;Foxg1* cKO cortices before E14.5 but gradually elevated afterward. Despite this expression rebound, note that at P0, FEZF2 showed a uniform expression pattern in SCPNs and CThPNs in *NEX-Cre;Foxg1* cKO cortices, rather than a SCPN^{high}CThPN^{low} pattern in the P0. Note that from E14.5 onward, both *Sox4* and *Sox11*, which have been reported to activate *Fzef2* transcription, were rebound in our cKO mice. These results suggest that (i) other regulatory mechanisms beyond *Fezf2* transcription are involved from E14.5 onward, and (ii) in the process of CFuNs diverging and developing into CThPNs or SCPNs, FOXG1 is required for the down-regulation of FEZF2 in the developing CThPNs and the accumulation of FEZF2 in the developing SCPNs. It seems likely that careful experimental characterization of FOXG1 and SOX protein binding competition at the *Fezf2* enhancer motif, especially around E14.5 to E16.5, as well as involvement of other mechanisms, could yield insights about the mechanism underlying SCPN versus CThPN fate.

FOXG1/BCL11B in CThPN and FOXG1/TBR1 in SCPN specification after E14.5

To achieve a TBR1^{high}BCL11B^{low} CThPN profile after E14.5, BCL11B must become reduced in CThPNs. The ectopic high expression of FEZF2/BCL11B in CThPNs can reverse their progression, ultimately directing them toward a SCPN fate (*16*, *32*, *63*). Our study found that FOXG1 is a negative regulator that directly represses BCL11B in CThPNs after E14.5.

To achieve a TBR1^{low}BCL11B^{high} SCPN pattern after E14.5, the TBR1 level needs to be reduced in developing SCPNs (*15*). Previous work showed an increase in TBR1^{+} CThPNs in *Ctip2*$^{-/-}$ mice, suggesting that BCL11B may repress TBR1 in SCPNs (*62*). Although we here show that FOXG1 is a repressor of *Tbr1* transcription in superficial CPNs, we found that FOXG1 does not repress *Tbr1* in SCPNs. Thus, our results are congruent with the previous proposal that BCL11B may function as a transcriptional repressor of *Tbr1* in SCPNs.

Specification of deep and superficial CPNs after E14.5

SATB2 is postmitotically highly expressed in both deep and superficial CPNs and contributes to specification of their identities (*14*, *36*). In *Fezf2*$^{-/-}$ mice, a marked accumulation of SATB2 is observed and SCPNs converged to CPNs, but there is no experimental evidence that FEZF2 directly regulates *Satb2* (*13*). The zinc finger and broad complex, tramtrack, bric-a-brac (BTB) domain–containing protein 20 (ZBTB20) was previously reported to repress CPN fate by repressing *Satb2* in the isocortex (*64*). Here, we have identified FOXG1 as an activator of *Satb2* and show that FOXG1 enforces the identities of both deep and superficial CPNs (Fig. 9). It will be interesting to explore whether FOXG1 antagonizes ZBTB20 to promote CPN identity.

Deep CPNs exhibit a SATB2^{high}BCL11B^{low}TBR1^{low} profile, whereas superficial CPNs display a SATB2^{high}BCL11B^{-}TBR1^{low} profile (*36*, *40*). In the present study, we found that after E14.5, FOXG1 directly represses *Bcl11b* in deep CPNs and that FOXG1 represses *Tbr1* in superficial CPNs. Our study therefore reveals mechanisms through which FOXG1 instructs the specification of two neuron subtypes that are quite morphologically and functionally distinct.

Impaired cortical projection neuron subtype specification and *FOXG1* syndrome

FOXG1 syndrome is a severe developmental encephalopathy characterized by autistic features including intellectual disability, limited language ability, and prominent movement disorders (*65*). It is also highly relevant that corpus callosum agenesis has been reported in *FOXG1* syndrome (*66*); corpus callosum agenesis is closely related to cognitive syndromes with high-level associative dysfunction (*6*). We know that dysfunction of CThPNs and SCPNs results in perceptual-motor dysfunction as well as attention deficit and hyperactivity (*2*, *3*). In the present study, extending beyond the molecular and neuronal developmental phenotypes toward direct clinical relevance, we detected multiple brain anatomy phenotypes in mice lacking *Foxg1* that mirror the human disorder *FOXG1* syndrome. Specifically, these mice have a severely disrupted corpus callosum (exhibiting an agenesis phenotype specifically affected by deep and superficial CPNs), as well as impaired corticothalamic tracts (related to CThPNs) and corticospinal tracts (related to SCPNs). Our study thus deepens understanding of the timing and molecular nature of the activation/repression transcription networks that control subtype specification for cortical projection neurons and sheds light on the pathogenesis *FOXG1*-associated dyskinesia and cognitive deficits and related neurodevelopmental disorders.

MATERIALS AND METHODS

Mice

Foxg1$^{fl/fl}$ mice and *CAG-loxp-stop-loxp-Foxg1-IRES-EGFP* mice were generated as previously described (*26*, *45*). *ROSA-Ai9-tdTomato* (stock no. 007905), *CAG-CreER* (stock no. 004453), and *Satb2-Cre-GFP mice* (stock no. 030546) were purchased from the Jackson Laboratory. *Ntsr1-Cre* mice (MMRRC:030648-UC) and *Rbp4-Cre* mice (MMRRC:037128-UCD) were purchased from the Mutant Mouse Regional Resource Centers (MMRRC) (*44*). *NEX-Cre* mice were previously described (*30*). *CAG-CreER;Foxg1*$^{fl/fl}$, *NEX-Cre;Foxg1*$^{fl/fl}$, *Ntsr1-Cre;Foxg1*$^{fl/fl}$, *Rbp4-Cre;Foxg1*$^{fl/fl}$, and *Satb2-Cre-GFP;Foxg1*$^{fl/fl}$ mice were referred to as *CAG-CreER;Foxg1* cKO, *NEX-Cre;Foxg1* cKO, *Ntsr1-Cre;Foxg1* cKO, *Rbp4-Cre;Foxg1* cKO, and *Satb2-Cre;Foxg1* cKO mice, respectively. *Foxg1*$^{fl/fl}$ mice were referred to as control mice. The day of the vaginal plug detection was assigned as E0.5. The day of birth was assigned as P0. Unless noted otherwise, all experiments were performed using mice maintained on a CD1 background. No significant differences based on sex were observed, and data were

pooled between sexes. All mouse studies were approved by the Southeast University Institutional Animal Care and Use Committee and were performed in accordance with institutional and national guidelines.

TM induction

TM (Sigma-Aldrich, catalog no. T5648) was dissolved in corn oil at the concentration of 20 mg/ml. Pregnant mice were dosed with TM (2 mg per 40 g of body weight) once at E14.5.

Cell tracing and immunofluorescence

For BrdU (Sigma-Aldrich, catalog no. B5002) labeling, timed pregnant females were intraperitoneally administered with 50 mg/kg body weight at E12.5, E13.5, and E15.5. Brains of paired littermates were examined at P0 (E12.5BrdU and E13.5BrdU) or P2 (E15.5BrdU). Briefly, mice were transcardially perfused with 4% paraformaldehyde (PFA), cryoprotected in 30% sucrose, and sectioned on a cryostat (Leica, CM 3050S). Immunofluorescence staining was performed as previously described (*67*): Briefly, sections were permeabilized in phosphate-buffered saline (PBS) containing 0.1% Triton X-100 for 0.5 hours, blocked with 10% calf serum for 2 hours, and incubated in primary antibody diluted in blocking solution overnight at 4°C. Sections were then incubated in secondary antibody for 2 hours at room temperature (RT). As for BrdU immunofluorescence, sections were fixed in 4% PFA for 20 min at RT after the aforementioned incubation and were treated with 2 N HCl at 37°C for 0.5 hours, rinsed three times in PBS, and then incubated with anti-BrdU antibody overnight at 4°C followed by secondary antibody incubation for 2 hours at RT. Images were captured with a confocal microscope (FluoView FV1000, Olympus).

In situ hybridization analyses

Digoxigenin (DIG) UTP (uridine 5′-triphosphate)–labeled riboprobes were used. The primers for probes are seen in table S1. Probes were obtained by PCR amplification. In situ hybridization was performed as previously described (*45*). Simply, E14.5 brains were dissected out and immersed in 4% diethyl pyrocarbonate (DEPC)–PFA overnight; E16.5 and P0 brains were transcardially perfused with 4% DEPC-PFA and fixed in 4% DEPC-PFA overnight. Brains were then cryoprotected in 30% sucrose/DEPC-PBS at 4°C. Brain sections were hybridized with digoxigenin-labeled antisense RNA probes at 65°C overnight, incubated with anti–digoxigenin–alkaline phosphatase antibody for 2 hours at RT, and then subjected to color development.

Western blotting analyses

Western blotting was performed according to a standard protocol (*68*). Cortex extracts at P0 were separated on 8% SDS–polyacrylamide gel electrophoresis gel and transferred to nitrocellulose membranes. The membranes were blocked for 2 hours in 10% nonfat dry milk containing 20 mM tris-HCl (pH 7.5), 150 mM NaCl, and 0.1% Tween 20 and incubated with primary antibodies overnight at 4°C followed by secondary horseradish peroxidase–linked anti-rabbit immunoglobulin G (IgG) incubation for 2 hours at RT. Proteins were detected using chemiluminescence SuperSignal West Dura kit (Thermo Fisher Scientific).

Retrograde tracing

For in vivo retrograde tracing, DiI (Invitrogen, catalog no. 1818465) was injected into the pyramid region of the medulla at P2 live mice under ice anesthesia (*39*). Brains were collected at P20.

RNA isolation, reverse transcription, and qPCR analysis

RNA isolation, reverse transcription, and qPCR were performed as previously described (*69*). Dorsal cortices were dissected from control mice over the developmental stages of E12.5 to P0. Total RNA was extracted using the RNeasy Plus Mini Kit (QIAGEN, 74104) and was reverse transcribed using the PrimeScript RT Reagent Kit with gDNA Eraser (Takara, RR047A). The qPCRs were performed using the SYBR Green fluorescent master mix (Roche, catalog no. 04707516001) on the Step One-Plus Real-Time PCR System (Applied Biosystems). Relative mRNA expression levels were normalized with the expression of glyceraldehyde 3-phosphate dehydrogenase (GAPDH). The primers for qPCR were designed with Integrated DNA Technologies (IDT; https://sg.idtdna.com) and are listed in table S1. At least three brains from three different litters were used, and samples were run in three duplicates of each sample. All of values were presented as means ± SEM.

Identification of FOXG1-binding sites

The binding sites of FOXG1 at *Fezf2* promotor and enhancer, and *Tbr1* promotor have been previously reported by Eckler *et al.* (*41*) and by Hanashima and co-workers (*43*). For picking up binding sites at transcription factors of *Sox5*, *Sox4*, *Sox11*, *Satb2*, and *Bcl11b*, we first scored a 10-kb upstream region of each transcription start site to predict its promoter domain using BDGP (Berkeley Drosophila Genome Project) (www.fruitfly.org/seq_tools/promoter.html) and Promoter 2.0 (https://services.healthtech.dtu.dk/service.php?Promoter-2.0). Next, we evaluated the conservation of the consensus binding sites of RYAAAYA of FOXG1 at each putative promotor locus across species at the UCSC database (http://genome.ucsc.edu/) as previously reported (*25*, *43*, *70*). Third, we scored the binding motifs in each putative promoter by JASPAR (https://jaspar.genereg.net/); high-score binding motifs were selected and were further compared with the ChIP-seq data reported by Cargnin *et al.* (*25*). Last, promotor domains with high-score binding motifs that were validated by the FOXG1-bound ChIP-seq peak data were selected for further ChIP-qPCR and luciferase assays. As for *Bcl11b*, we identified a repressor site containing FOXG1-binding motifs using the VISTER Enhancer Browser (http://enhancer.lbl.gov/), which we compared with the ChIP-seq data reported by Cargnin *et al.* (*25*).

ChIP-qPCR analyses

ChIP was performed as described previously using an EZ-Magna ChIP A/G kit (Millipore, catalog no. 17-10086) (*71*). Briefly, dorsal cortices from E14.5 were mechanically homogenized, and samples were cross-linked with 1% formaldehyde for 15 min and quenched with 125 mM glycine. The chromatin was sheared into 200 to 1000 base pairs for immunoprecipitation using 3 μg of rabbit antibodies against FOXG1, and an equal amount of rabbit IgG was applied as negative control. One percent unimmunoprecipitated input DNA served as internal control. After cross-linking was reversed, immunoprecipitated DNA and input DNA were purified for qPCR analyses. The primers for qPCR were designed with IDT and are listed in table S1. All experiments were run in three duplicates and repeated at least three independent times. ChIP-qPCR data were normalized to the amount of chromatin input. The percentage of input was calculated as follows: % of input = $1\% \times 2^{-\Delta Ct}$ (C[T] IP sample − C[T] input sample). C[T] = CT = average threshold cycle of PCR. The values were presented as means ± SEM.

Luciferase assay

The luciferase assay was performed as previous described (*22*, *71*). Overexpression vectors of *pCAG-Foxg1* (mouse; NM_008241), *pCAG-Sox4* (mouse; NM_009238), *pCAG-Sox5* (mouse; AB006330), and *pCAG-Sox11* (mouse; NM_009234) were customized from Synbio Technologies (www.synbio-tech.com; Beijing, China). Reporter vectors of *pGL3-Fezf2-Pro* (chr14:13177700-13181294), *pGL3-Fezf2-En* (chr14:13170122-13170950), *pGL3-Sox4-Pro* (crh13:29045352-29047551), *pGL3-Sox5-Pro* (crh6:144157589-144160688), *pGL3-Sox11-Pro* (crh12:28027000-2809583), *pGL3-Satb2-Pro* (chr1:57026666-57030006), and *pGL3-Bcl11b-rep* (chr12: 109189361-109192204) were customized from GENEWIZ (www.Genewiz.com; Nanjing, China). *pGL3-Tbr1-Pro* (chr2: 61638039-61642764) was homemade, in which the promoter fragment of *Tbr1* amplified by PCR was subcloned into the *pGL3* basic vector between 5′ Nhe I and 3′ Hind III. CE Design V1.04 was used for primer design (Vazyme, Nanjing, China). Homologous recombination was performed with the ClonExpress II One Step Cloning Kit (Vazyme, catalog no. C112-01). The reporters in which the FOXG1-binding motifs were deleted/point mutated were generated using the Mut Express II Fast Mutagenesis Kit V2 (Vazyme, catalog no. C214-01). Deletion/mutation information is presented in table S3. All of the constructs were verified by sequencing.

Neuro2a cells [RRID (Research Resource Identifiers): CVCL0470; The Cell Bank of the Chinese Academy of Science, Shanghai, China] were cultured in Dulbecco's modified Eagle's medium (DMEM)/F12 (Thermo Fisher Scientific, catalog no. 11320082) supplemented with 10% (v/v) fetal bovine serum (Thermo Fisher Scientific, catalog no. 10099141C), penicillin (100 U/ml), and streptomycin (100 μg/ml) (Millipore, catalog no. 516104-M). A total of 1×10^{-5} cells per cell were seeded for transfection. The transfection complex was prepared including the *pCAG* vector (control) or overexpression vectors (250 ng per cell), control or mutation reporter vector (200 ng per cell), *pRL-SV40* plasmid containing *Renilla* luciferase gene (25 ng per cell), and Lipofectamine 2000 (2.5 μl per cell) (Thermo Fisher Scientific, catalog no. 11668-019). For normalization of luciferase activity, the *pRL-SV40* vector encoding *Renilla* luciferase was used as an internal control reporter and was used in combination with any experimental reporter vector to cotransfect mammalian cells. The cells were harvested 24 hours after transfection. Firefly and *Renilla* luciferase activities were measured using the Dual Luciferase Reporter Assay System (Promega, E1910). The ratio of Firefly luciferase readouts and *Renilla* luciferase readout was calculated to represent the activity of the reporter vector. Three replicate wells were made for each transfection. Each experiment was repeated at least three times, and all results are shown as means ± SEM.

In utero electroporation

For in utero electroporation, timed-pregnant *Foxg1*$^{fl/fl}$ females (E12.5) were deeply anesthetized, and embryos were surgically manipulated as described previously (*72*). Plasmids encoding GFP only (*pNeuroD1-IRES-GFP*) or *Cre-GFP* (*pNeuroD1-Cre-HA- IRES-GFP*) (2 μg/μl) (*37*) were injected directly into the lateral ventricles and electroporated with paddle electrodes across the cerebrum. Electroporation was performed using Tweezertrodes (diameter of 5 mm; BTX) with five pulses (30 V for E12.5 embryos) for 50-ms duration and 950-ms intervals using a square-wave pulse generator (ECM830, BTX). The uterus was then returned to the abdominal cavity, and the inner skin and outer skin were sutured. Surgically manipulated pregnant mice were then put on an electric heating plate (50°C) until they awoke. Progenies were euthanized at E18.5 for analysis. Three pairs of control and *Foxg1* knockdown brains were analyzed.

Quantification of histological analyses

The confocal images were acquired by FluoView FV1000 confocal microscopy (Olympus) with 20× objective lens. A minimum of three successive coronal sections crossing the somatosensory cortex were selected. Quantitative analyses of neurons were consistently performed in the same area in the somatosensory cortex by direct comparisons of brain sections. At least three brains of each genotype from three different litters were used. The experiments of cell counting were all cross-quantified blindly (i.e., the investigator was unaware of the genotypes). All results are shown as means ± SEM, except indicated otherwise. GraphPad Prism 7 software was used for statistical analyses, and multiple *t* test with Bonferroni correction and unpaired Student's *t* test were used for two-group comparisons. The following convention was used: *$P < 0.05$; **$P < 0.01$; ***$P < 0.001$; ****$P < 0.0001$; ns, not significant.

In Fig. 1 (F to H), to measure SATB2^{high} and BCL11B^{high}TBR1^{high} cells in the control and *NEX-Cre;Foxg1* cKO cortices, a square box spanning the marginal zone to the white matter of the somatosensory cortex was overlaid, and all SATB2^{high} and BCL11B^{high}TBR1^{high} neurons within the box were quantified. In detail, cells in a box of 180 μm by 360 μm at E14.5, 180 μm by 420 μm at E16.5, and 300 μm by 500 μm at P0 were quantified with Image-Pro Plus software (Media Cybernetics).

In Fig. 2H, to measure TBR1^{high}, BCL11B^{high}TBR1^{high}, SATB^{high}, and BCL11B^{high} neurons at P0 in control and *CAG-CreER;Foxg1* cKO, a box of 175 μm by 500 μm in the somatosensory cortex was overlaid. The upper boundary of BCL11B^{+} neurons was used to demarcate the superficial and deep layers, and neurons in the deep layer within the box were counted.

In Fig. 3 (G to I) and fig. S5 (C and D), cell tracing was performed to detect subtype specification. Only the first-generation wave of BrdU^{+} neurons with strong and homogeneous nuclear labeling was counted. BrdU^{+}, SATB^{high}BrdU^{+}, BCL11B^{high}BrdU^{+}, and TBR1^{high}BrdU^{+} neurons in the entire cortex were counted in a box of 175 μm by 500 μm at P0 (for E12.5BrdU and E13.5BrdU labeling) and a box of 175 μm by 600 μm at P2 (for E15.5BrdU labeling). The proportions of SATB^{high} BrdU^{+}, BCL11B^{high} BrdU^{+}, and TBR1^{high} BrdU^{+} neurons among total BrdU^{+} neurons were calculated.

In Fig. 7E, to measure TBR1^{high}BCL11B^{low} and TBR1^{high}BCL11B^{high} neurons in control and *Ntsr1-Cre;Foxg1* cKO cortices, a box of 300 μm by 800 μm in the somatosensory cortex was overlaid. All neurons in L6 in this box were quantified. In Fig. 7F, to measure tdTom^{+}, SATB2^{+}tdTom^{+}, BCL11B^{+}tdTom^{+}, and TBR1^{+}tdTom^{+} neurons in control and *Rbp4-Cre;Foxg1* cKO cortices, a box of 300 μm by 800 μm in the somatosensory cortex was overlaid. All tdTom^{+}, SATB2^{+}tdTom^{+}, BCL11B^{+}tdTom^{+}, and TBR1^{+}tdTom^{+} neurons in this box were quantified, and the ratios of SATB2^{+}tdTom^{+}, BCL11B^{+}tdTom^{+}, and TBR1^{+}tdTom^{+} neurons in tdTom^{+} neurons were calculated.

In fig. S3C, all GFP^{+}, SATB2^{+}GFP^{+}, BCL11B^{+}GFP^{+}, and TBR1^{+}GFP^{+} neurons in the cortices of three pairs of control and *Foxg1* knockdown brains were measured, and the ratios of SATB2^{+}GFP^{+}, BCL11B^{+}GFP^{+}, and TBR1^{+}GFP^{+} neurons in GFP^{+} neurons were calculated. In fig. S6, to measure PKC-γ^{+} neurons in control and *CAG-CreER;Foxg1* cKO brains at P8, a box of 300 μm by 800 μm was overlaid, and all labeled neurons within the box were quantified.

Quantification of fluorescence intensity

Immunostaining was performed as described above. Sections were imaged with the same confocal acquisition parameters at the same level for each of the individual protein assessed with immunostaining. The mean fluorescence intensities were analyzed using the FV10-ASW4.2 software, with the same settings. All results are shown as means ± SEM. GraphPad Prism 7 software was used for statistical analyses, and unpaired Student's *t* test was used for two-group comparisons. The following convention was used: $*P < 0.05$; $**P < 0.01$; $***P < 0.001$; $****P < 0.0001$; ns, not significant.

In fig. S2, the mean fluorescence intensities of FOXG1 in deep SATB2^{high} CPNs and BCL11B^{high} CFuNs in CP were measured. At least 200 neurons at E14.5 and E16.5 were measured. Two control brains were analyzed at each time point.

In fig. S9, the mean fluorescence intensities of FOXG1, SATB2, BCL11B, or TBR1 in SCPNs and CThPNs were measured. Two pairs of E18.5 brains from control versus *NEX-Cre;CAG-Foxg1* TG mice were analyzed. At least 200 neurons for each population were analyzed.

In Fig. 8, the mean fluorescence intensities of BCL11B in deep CPNs and TBR1 in superficial CPNs were measured. Two pairs of E18.5 brains from control versus *Satb2-Cre;Foxg1* cKO mice were used, and at least 450 neurons were analyzed for each population.

Statistical analysis for ChIP-qPCR and luciferase assay

The data of ChIP-qPCR were analyzed with unpaired Student's *t* test for two-group comparisons [Figs. 4 (F and G), 5 (D to F), and 6 (B, F, and J)]. The data of the luciferase assay were analyzed with one-way analysis of variance (ANOVA) followed by Tukey-Kramer post hoc test for multiple-group cotransfection tests [Figs. 4 (I and J), 5 (D to I and L to N), and 6 (C, G, and K)].

SUPPLEMENTARY MATERIALS

Supplementary material for this article is available at https://science.org/doi/10.1126/sciadv.abh3568

View/request a protocol for this paper from *Bio-protocol*.

REFERENCES AND NOTES

1. S. Lodato, A. S. Shetty, P. Arlotta, Cerebral cortex assembly: Generating and reprogramming projection neuron diversity. *Trends Neurosci.* **38**, 117–125 (2015).
2. Q. Welniarz, I. Dusart, E. Roze, The corticospinal tract: Evolution, development, and human disorders. *Dev. Neurobiol.* **77**, 810–829 (2017).
3. R. Yuste, M. Hawrylycz, N. Aalling, A. Aguilar-Valles, D. Arendt, R. Armañanzas, G. A. Ascoli, C. Bielza, V. Bokharaie, T. B. Bergmann, I. Bystron, M. Capogna, Y. J. Chang, A. Clemens, C. P. J. de Kock, J. DeFelipe, S. E. Dos Santos, K. Dunville, D. Feldmeyer, R. Fiáth, G. J. Fishell, A. Foggetti, X. Gao, P. Ghaderi, N. A. Goriounova, O. Güntürkün, K. Hagihara, V. J. Hall, M. Helmstaedter, S. Herculano-Houzel, M. M. Hilscher, H. Hirase, J. Hjerling-Leffler, R. Hodge, J. Huang, R. Huda, K. Khodosevich, O. Kiehn, H. Koch, E. S. Kuebler, M. Kühnemund, P. Larrañaga, B. Lelieveldt, E. L. Louth, J. H. Lui, H. D. Mansvelder, O. Marin, J. Martinez-Trujillo, H. M. Chameh, A. N. Mohapatra, H. Munguba, M. Nedergaard, P. Němec, N. Ofer, U. G. Pfisterer, S. Pontes, W. Redmond, J. Rossier, J. R. Sanes, R. H. Scheuermann, E. Serrano-Saiz, J. F. Staiger, P. Somogyi, G. Tamás, A. S. Tolias, M. A. Tosches, M. T. García, C. Wozny, T. V. Wuttke, Y. Liu, J. Yuan, H. Zeng, E. Lein, A community-based transcriptomics classification and nomenclature of neocortical cell types. *Nat. Neurosci.* **23**, 1456–1468 (2020).
4. M. Avram, F. Brandl, J. Bauml, C. Sorg, Cortico-thalamic hypo- and hyperconnectivity extend consistently to basal ganglia in schizophrenia. *Neuropsychopharmacology* **43**, 2239–2248 (2018).
5. R. M. Fame, J. L. MacDonald, J. D. Macklis, Development, specification, and diversity of callosal projection neurons. *Trends Neurosci.* **34**, 41–50 (2011).
6. W. S. Brown, L. K. Paul, The neuropsychological syndrome of agenesis of the corpus callosum. *J. Int. Neuropsychol. Soc.* **25**, 324–330 (2019).
7. N. S. De Leon Reyes, L. Bragg-Gonzalo, M. Nieto, Development and plasticity of the corpus callosum. *Development* **147**, (2020).
8. L. C. Greig, M. B. Woodworth, M. J. Galazo, H. Padmanabhan, J. D. Macklis, Molecular logic of neocortical projection neuron specification, development and diversity. *Nat. Rev. Neurosci.* **14**, 755–769 (2013).
9. M. Shibata, F. O. Gulden, N. Sestan, From trans to cis: Transcriptional regulatory networks in neocortical development. *Trends Genet.* **31**, 77–87 (2015).
10. A. Paolino, L. R. Fenlon, R. Suarez, L. J. Richards, Transcriptional control of long-range cortical projections. *Curr. Opin. Neurobiol.* **53**, 57–65 (2018).
11. C. Rouaux, S. Bhai, P. Arlotta, Programming and reprogramming neuronal subtypes in the central nervous system. *Dev. Neurobiol.* **72**, 1085–1098 (2012).
12. D. P. Leone, K. Srinivasan, B. Chen, E. Alcamo, S. K. McConnell, The determination of projection neuron identity in the developing cerebral cortex. *Curr. Opin. Neurobiol.* **18**, 28–35 (2008).
13. B. Chen, S. S. Wang, A. M. Hattox, H. Rayburn, S. B. Nelson, S. K. McConnell, The Fezf2-Ctip2 genetic pathway regulates the fate choice of subcortical projection neurons in the developing cerebral cortex. *Proc. Natl. Acad. Sci. U.S.A.* **105**, 11382–11387 (2008).
14. E. A. Alcamo, L. Chirivella, M. Dautzenberg, G. Dobreva, I. Fariñas, R. Grosschedl, S. K. McConnell, Satb2 regulates callosal projection neuron identity in the developing cerebral cortex. *Neuron* **57**, 364–377 (2008).
15. B. J. Molyneaux, P. Arlotta, T. Hirata, M. Hibi, J. D. Macklis, Fezl is required for the birth and specification of corticospinal motor neurons. *Neuron* **47**, 817–831 (2005).
16. W. L. McKenna, J. Betancourt, K. A. Larkin, B. Abrams, C. Guo, J. L. R. Rubenstein, B. Chen, Tbr1 and Fezf2 regulate alternate corticofugal neuronal identities during neocortical development. *J. Neurosci.* **31**, 549–564 (2011).
17. J. G. Chen, M. R. Rasin, K. Y. Kwan, N. Sestan, Zfp312 is required for subcortical axonal projections and dendritic morphology of deep-layer pyramidal neurons of the cerebral cortex. *Proc. Natl. Acad. Sci. U.S.A.* **102**, 17792–17797 (2005).
18. B. Chen, L. R. Schaevitz, S. K. McConnell, Fezl regulates the differentiation and axon targeting of layer 5 subcortical projection neurons in cerebral cortex. *Proc. Natl. Acad. Sci. U.S.A.* **102**, 17184–17189 (2005).
19. P. Arlotta, B. J. Molyneaux, J. Chen, J. Inoue, R. Kominami, J. D. Macklis, Neuronal subtype-specific genes that control corticospinal motor neuron development in vivo. *Neuron* **45**, 207–221 (2005).
20. S. Shim, K. Y. Kwan, M. Li, V. Lefebvre, N. Sestan, Cis-regulatory control of corticospinal system development and evolution. *Nature* **486**, 74–79 (2012).
21. T. Lai, D. Jabaudon, B. J. Molyneaux, E. Azim, P. Arlotta, J. R. L. Menezes, J. D. Macklis, SOX5 controls the sequential generation of distinct corticofugal neuron subtypes. *Neuron* **57**, 232–247 (2008).
22. K. Y. Kwan, M. M. S. Lam, Ž. Krsnik, Y. I. Kawasawa, V. Lefebvre, N. Šestan, SOX5 postmitotically regulates migration, postmigratory differentiation, and projections of subplate and deep-layer neocortical neurons. *Proc. Natl. Acad. Sci. U.S.A.* **105**, 16021–16026 (2008).
23. S. Xuan, C. A. Baptista, G. Balas, W. Tao, V. C. Soares, E. Lai, Winged helix transcription factor BF-1 is essential for the development of the cerebral hemispheres. *Neuron* **14**, 1141–1152 (1995).
24. G. Miyoshi, G. Fishell, Dynamic FoxG1 expression coordinates the integration of multipolar pyramidal neuron precursors into the cortical plate. *Neuron* **74**, 1045–1058 (2012).
25. F. Cargnin, J.-S. Kwon, S. Katzman, B. Chen, J. W. Lee, S.-K. Lee, FOXG1 orchestrates neocortical organization and cortico-cortical connections. *Neuron* **100**, 1083–1096.e5 (2018).
26. C. Tian, Y. Gong, Y. Yang, W. Shen, K. Wang, J. Liu, B. Xu, J. Zhao, C. Zhao, Foxg1 has an essential role in postnatal development of the dentate gyrus. *J. Neurosci.* **32**, 2931–2949 (2012).
27. C. Hanashima, S. C. Li, L. Shen, E. Lai, G. Fishell, Foxg1 suppresses early cortical cell fate. *Science* **303**, 56–59 (2004).
28. J. Seoane, H. V. Le, L. Shen, S. A. Anderson, J. Massague, Integration of Smad and forkhead pathways in the control of neuroepithelial and glioblastoma cell proliferation. *Cell* **117**, 211–223 (2004).
29. N. Vegas, M. Cavallin, C. Maillard, N. Boddaert, J. Toulouse, E. Schaefer, T. Lerman-Sagie, D. Lev, B. Magalie, S. Moutton, E. Haan, B. Isidor, D. Heron, M. Milh, S. Rondeau, C. Michot, S. Valence, S. Wagner, M. Hully, C. Mignot, A. Masurel, A. Datta, S. Odent, M. Nizon, L. Lazaro, M. Vincent, B. Cogné, A. M. Guerrot, S. Arpin, J. M. Pedespan, I. Caubel, B. Pontier, B. Troude, F. Rivier, C. Philippe, T. Bienvenu, M. A. Spitz, A. Bery, N. Bahi-Buisson, Delineating FOXG1 syndrome: From congenital microcephaly to hyperkinetic encephalopathy. *Neurol Genet* **4**, e281 (2018).
30. S. Goebbels, I. Bormuth, U. Bode, O. Hermanson, M. H. Schwab, K. A. Nave, Genetic targeting of principal neurons in neocortex and hippocampus of NEX-Cre mice. *Genesis* **44**, 611–621 (2006).
31. J. R. Lu, T. A. McKinsey, H. Xu, D. Z. Wang, J. A. Richardson, E. N. Olson, FOG-2, a heart- and brain-enriched cofactor for GATA transcription factors. *Mol. Cell. Biol.* **19**, 4495–4502 (1999).
32. M. J. Galazo, J. G. Emsley, J. D. Macklis, Corticothalamic projection neuron development beyond subtype specification: Fog2 and intersectional controls regulate intraclass neuronal diversity. *Neuron* **91**, 90–106 (2016).
33. B. Cubelos, A. Sebastián-Serrano, L. Beccari, M. E. Calcagnotto, E. Cisneros, S. Kim, A. Dopazo, M. Alvarez-Dolado, J. M. Redondo, P. Bovolenta, C. A. Walsh, M. Nieto, Cux1 and Cux2 regulate dendritic branching, spine morphology, and synapses of the upper layer neurons of the cortex. *Neuron* **66**, 523–535 (2010).

34. O. Britanova, S. Akopov, S. Lukyanov, P. Gruss, V. Tarabykin, Novel transcription factor Satb2 interacts with matrix attachment region DNA elements in a tissue-specific manner and demonstrates cell-type-dependent expression in the developing mouse CNS. *Eur. J. Neurosci.* **21**, 658–668 (2005).
35. D. J. Dennis, G. Wilkinson, S. Li, R. Dixit, L. Adnani, A. Balakrishnan, S. Han, C. Kovach, N. Gruenig, D. M. Kurrasch, R. H. Dyck, C. Schuurmans, *Neurog2* and *Ascl1* together regulate a postmitotic derepression circuit to govern laminar fate specification in the murine neocortex. *Proc. Natl. Acad. Sci. U.S.A.* **114**, E4934–E4943 (2017).
36. O. Britanova, C. de Juan Romero, A. Cheung, K. Y. Kwan, M. Schwark, A. Gyorgy, T. Vogel, S. Akopov, M. Mitkovski, D. Agoston, N. Šestan, Z. Molnár, V. Tarabykin, Satb2 is a postmitotic determinant for upper-layer neuron specification in the neocortex. *Neuron* **57**, 378–392 (2008).
37. C. Wei, M. Sun, X. Sun, H. Meng, Q. Li, K. Gao, W. Yue, L. Wang, D. Zhang, J. Li, RhoGEF trio regulates radial migration of projection neurons via its distinct domains. *Neurosci. Bull.* **38**, 249–262 (2022).
38. S. Guerrier, J. Coutinho-Budd, T. Sassa, A. Gresset, N. V. Jordan, K. Chen, W. L. Jin, A. Frost, F. Polleux, The F-BAR domain of srGAP2 induces membrane protrusions required for neuronal migration and morphogenesis. *Cell* **138**, 990–1004 (2009).
39. W. Han, K. Y. Kwan, S. Shim, M. M. S. Lam, Y. Shin, X. Xu, Y. Zhu, M. Li, N. Šestan, TBR1 directly represses Fezf2 to control the laminar origin and development of the corticospinal tract. *Proc. Natl. Acad. Sci. U.S.A.* **108**, 3041–3046 (2011).
40. F. Bedogni, R. D. Hodge, G. E. Elsen, B. R. Nelson, R. A. M. Daza, R. P. Beyer, T. K. Bammler, J. L. R. Rubenstein, R. F. Hevner, Tbr1 regulates regional and laminar identity of postmitotic neurons in developing neocortex. *Proc. Natl. Acad. Sci. U.S.A.* **107**, 13129–13134 (2010).
41. M. J. Eckler, K. A. Larkin, W. L. McKenna, S. Katzman, C. Guo, R. Roque, A. Visel, J. L. L. Rubenstein, B. Chen, Multiple conserved regulatory domains promote Fezf2 expression in the developing cerebral cortex. *Neural Dev.* **9**, 6 (2014).
42. W. Tao, E. Lai, Telencephalon-restricted expression of BF-1, a new member of the HNF-3/fork head gene family, in the developing rat brain. *Neuron* **8**, 957–966 (1992).
43. K. Toma, T. Kumamoto, C. Hanashima, The timing of upper-layer neurogenesis is conferred by sequential derepression and negative feedback from deep-layer neurons. *J. Neurosci.* **34**, 13259–13276 (2014).
44. S. Gong, M. Doughty, C. R. Harbaugh, A. Cummins, M. E. Hatten, N. Heintz, C. R. Gerfen, Targeting Cre recombinase to specific neuron populations with bacterial artificial chromosome constructs. *J. Neurosci.* **27**, 9817–9823 (2007).
45. B. Liu, K. Zhou, X. Wu, C. Zhao, Foxg1 deletion impairs the development of the epithalamus. *Mol. Brain* **11**, 5 (2018).
46. B. C. Jarvie, J. Y. Chen, H. O. King, R. D. Palmiter, Satb2 neurons in the parabrachial nucleus mediate taste perception. *Nat. Commun.* **12**, 224 (2021).
47. R. Bassel-Duby, M. D. Hernandez, Q. Yang, J. M. Rochelle, M. F. Seldin, R. S. Williams, Myocyte nuclear factor, a novel winged-helix transcription factor under both developmental and neural regulation in striated myocytes. *Mol. Cell. Biol.* **14**, 4596–4605 (1994).
48. N. Bredenkamp, C. Seoighe, N. Illing, Comparative evolutionary analysis of the FoxG1 transcription factor from diverse vertebrates identifies conserved recognition sites for microRNA regulation. *Dev. Genes Evol.* **217**, 227–233 (2007).
49. X. Xie, M. J. T. Stubbington, J. K. Nissen, K. G. Andersen, D. Hebenstreit, S. A. Teichmann, A. G. Betz, The regulatory T cell lineage factor Foxp3 regulates gene expression through several distinct mechanisms mostly independent of direct DNA binding. *PLOS Genet.* **11**, e1005251 (2015).
50. J. Yao, E. Lai, S. Stifani, The winged-helix protein brain factor 1 interacts with groucho and hes proteins to repress transcription. *Mol. Cell. Biol.* **21**, 1962–1972 (2001).
51. N. Marcal, H. Patel, Z. Dong, S. Belanger-Jasmin, B. Hoffman, C. D. Helgason, J. Dang, S. Stifani, Antagonistic effects of Grg6 and Groucho/TLE on the transcription repression activity of brain factor 1/FoxG1 and cortical neuron differentiation. *Mol. Cell. Biol.* **25**, 10916–10929 (2005).
52. K. Tan, A. L. Shaw, B. Madsen, K. Jensen, J. Taylor-Papadimitriou, P. S. Freemont, Human PLU-1 has transcriptional repression properties and interacts with the developmental transcription factors BF-1 and PAX9. *J. Biol. Chem.* **278**, 20507–20513 (2003).
53. C. Hanashima, L. Shen, S. C. Li, E. Lai, Brain factor-1 controls the proliferation and differentiation of neocortical progenitor cells through independent mechanisms. *J. Neurosci.* **22**, 6526–6536 (2002).
54. T. Kumamoto, K. I. Toma, Gunadi, W. L. McKenna, T. Kasukawa, S. Katzman, B. Chen, C. Hanashima, Foxg1 coordinates the switch from nonradially to radially migrating glutamatergic subtypes in the neocortex through spatiotemporal repression. *Cell Rep.* **3**, 931–945 (2013).
55. G. Miyoshi, Y. Ueta, A. Natsubori, K. Hiraga, H. Osaki, Y. Yagasaki, Y. Kishi, Y. Yanagawa, G. Fishell, R. P. Machold, M. Miyata, FoxG1 regulates the formation of cortical GABAergic circuit during an early postnatal critical period resulting in autism spectrum disorder-like phenotypes. *Nat. Commun.* **12**, 3773 (2021).
56. P. S. Hou, G. Miyoshi, C. Hanashima, Sensory cortex wiring requires preselection of short- and long-range projection neurons through an Egr-Foxg1-COUP-TFI network. *Nat. Commun.* **10**, 3581 (2019).
57. R. Smith, Y. T. Huang, T. Tian, D. Vojtasova, O. Mesalles-Naranjo, S. M. Pollard, T. Pratt, D. J. Price, V. Fotaki, The transcription factor Foxg1 promotes optic fissure closure in the mouse by suppressing Wnt8b in the Nasal Optic Stalk. *J. Neurosci.* **37**, 7975–7993 (2017).
58. R. Vezzali, S. C. Weise, N. Hellbach, V. Machado, S. Heidrich, T. Vogel, The FOXG1/FOXO/SMAD network balances proliferation and differentiation of cortical progenitors and activates Kcnh3 expression in mature neurons. *Oncotarget* **7**, 37436–37455 (2016).
59. B. Martynoga, H. Morrison, D. J. Price, J. O. Mason, Foxg1 is required for specification of ventral telencephalon and region-specific regulation of dorsal telencephalic precursor proliferation and apoptosis. *Dev. Biol.* **283**, 113–127 (2005).
60. F. Liu, G. C. Hon, G. R. Villa, K. M. Turner, S. Ikegami, H. Yang, Z. Ye, B. Li, S. Kuan, A. Y. Lee, C. Zanca, B. Wei, G. Lucey, D. Jenkins, W. Zhang, C. L. Barr, F. B. Furnari, T. F. Cloughesy, W. H. Yong, T. C. Gahman, A. K. Shiau, W. K. Cavenee, B. Ren, P. S. Mischel, EGFR mutation promotes glioblastoma through epigenome and transcription factor network remodeling. *Mol. Cell* **60**, 307–318 (2015).
61. N. Buttner, S. A. Johnsen, S. Kugler, T. Vogel, Af9/Mllt3 interferes with Tbr1 expression through epigenetic modification of histone H3K79 during development of the cerebral cortex. *Proc. Natl. Acad. Sci. U.S.A.* **107**, 7042–7047 (2010).
62. K. Srinivasan, D. P. Leone, R. K. Bateson, G. Dobreva, Y. Kohwi, T. Kohwi-Shigematsu, R. Grosschedl, S. K. McConnell, A network of genetic repression and derepression specifies projection fates in the developing neocortex. *Proc. Natl. Acad. Sci. U.S.A.* **109**, 19071–19078 (2012).
63. G. S. Tomassy, E. de Leonibus, D. Jabaudon, S. Lodato, C. Alfano, A. Mele, J. D. Macklis, M. Studer, Area-specific temporal control of corticospinal motor neuron differentiation by COUP-TFI. *Proc. Natl. Acad. Sci. U.S.A.* **107**, 3576–3581 (2010).
64. J. V. Nielsen, M. Thomassen, K. Mollgard, J. Noraberg, N. A. Jensen, Zbtb20 defines a hippocampal neuronal identity through direct repression of genes that control projection neuron development in the isocortex. *Cereb. Cortex* **24**, 1216–1229 (2014).
65. P. S. Hou, D. O. hAilin, T. Vogel, C. Hanashima, Transcription and beyond: Delineating FOXG1 function in cortical development and disorders. *Front Cell Neurosci* **14**, 35 (2020).
66. F. Kortum, S. Das, M. Flindt, D. J. Morris-Rosendahl, I. Stefanova, A. Goldstein, D. Horn, E. Klopocki, G. Kluger, P. Martin, A. Rauch, A. Roumer, S. Saitta, L. E. Walsh, D. Wieczorek, G. Uyanik, K. Kutsche, W. B. Dobyns, The core FOXG1 syndrome phenotype consists of postnatal microcephaly, severe mental retardation, absent language, dyskinesia, and corpus callosum hypogenesis. *J. Med. Genet.* **48**, 396–406 (2011).
67. Y. Pan, Z. Jiang, D. Sun, Z. Li, Y. Pu, D. Wang, A. Huang, C. He, L. Cao, Cyclin-dependent kinase 18 promotes oligodendrocyte precursor cell differentiation through activating the extracellular signal-regulated kinase signaling pathway. *Neurosci. Bull.* **35**, 802–814 (2019).
68. J. Zhou, X. Zhang, Y. Zhou, B. Wu, Z. Y. Tan, Up-regulation of P2X7 receptors contributes to spinal microglial activation and the development of pain induced by BmK-I. *Neurosci. Bull.* **35**, 624–636 (2019).
69. W. Shen, R. Ba, Y. Su, Y. Ni, D. Chen, W. Xie, S. J. Pleasure, C. Zhao, Foxg1 regulates the postnatal development of cortical interneurons. *Cereb. Cortex* **29**, 1547–1560 (2019).
70. S. Dai, J. Li, H. Zhang, X. Chen, M. Guo, Z. Chen, Y. Chen, Structural basis for DNA recognition by FOXG1 and the characterization of disease-causing FOXG1 mutations. *J. Mol. Biol.* **432**, 6146–6156 (2020).
71. A. Du, X. Wu, H. Chen, Q.-R. Bai, X. Han, B. Liu, X. Zhang, Z. Ding, Q. Shen, C. Zhao, Foxg1 directly represses Dbx1 to confine the POA and subsequently regulate ventral telencephalic patterning. *Cereb. Cortex* **29**, 4968–4981 (2019).
72. F. Yang, A. Hu, Y. Guo, J. Wang, D. Li, X. Wang, S. Jin, B. Yuan, S. Cai, Y. Zhou, Q. Li, G. Chen, H. Gao, L. Zheng, Q. Tong, p113 isoform encoded by CUX1 circular RNA drives tumor progression via facilitating ZRF1/BRD4 transactivation. *Mol. Cancer* **20**, 123 (2021).

Acknowledgments: We thank M. Fang, C. Lin, and J. Li at Southeast University, as well as S. J. Pleasure at UCSF for insightful comments and suggestions. We thank D. Zhang at Peking University for gift of pNeuroD1 plasmid. We thank Y. Wei and L. Liu for assistance with laboratory and animal care, and other members of the laboratory for discussions. **Funding:** The National Natural Science Foundation of China grant 31930045, major projects of the Ministry of Science and Technology of China 2021ZD0202304, and National Natural Science Foundation of China grant 81870899. **Author contributions:** Conceptualization: C.Z. and J.L. Methodology: C.Z. and J.L. Investigation: J.L., M.Y., M.S., B.L., K.Z., C.S., R.B., B.Y., R.B., B.Z., Z.Z., W.F., K.W., M.Z., and J.H. Visualization: J.L. Supervision: C.Z. Writing—original draft: C.Z. and J.L. Writing—review and editing: C.Z. **Competing interests:** The authors declare that they have no competing interests. **Data and materials availability:** All data needed to evaluate the conclusions in the paper are present in the paper and/or the Supplementary Materials.

Submitted 5 March 2021
Accepted 8 April 2022
Published 25 May 2022
10.1126/sciadv.abh3568